INFORMATION TO USERS

The most advanced technology has been used to photograph and reproduce this manuscript from the microfilm master. UMI films the text directly from the original or copy submitted. Thus, some thesis and dissertation copies are in typewriter face, while others may be from any type of computer printer.

The quality of this reproduction is dependent upon the quality of the copy submitted. Broken or indistinct print, colored or poor quality illustrations and photographs, print bleedthrough, substandard margins, and improper alignment can adversely affect reproduction.

In the unlikely event that the author did not send UMI a complete manuscript and there are missing pages, these will be noted. Also, if unauthorized copyright material had to be removed, a note will indicate the deletion.

Oversize materials (e.g., maps, drawings, charts) are reproduced by sectioning the original, beginning at the upper left-hand corner and continuing from left to right in equal sections with small overlaps. Each original is also photographed in one exposure and is included in reduced form at the back of the book. These are also available as one exposure on a standard 35mm slide or as a 17" x 23" black and white photographic print for an additional charge.

Photographs included in the original manuscript have been reproduced xerographically in this copy. Higher quality 6" x 9" black and white photographic prints are available for any photographs or illustrations appearing in this copy for an additional charge. Contact UMI directly to order.

UMI

University Microfilms International
A Bell & Howell Information Company
300 North Zeeb Road, Ann Arbor, MI 48106-1346 USA
313/761-4700 800/521-0600

Order Number 1336557

Three-dimensional incoherent optical transfer function in the presence of third-order spherical aberration

Wang, Shu-i, M.S.

The University of Arizona, 1989

U·M·I
300 N. Zeeb Rd.
Ann Arbor, MI 48106

THREE-DIMENSIONAL INCOHERENT OPTICAL TRANSFER FUNCTION IN THE PRESENCE OF THIRD-ORDER SPHERICAL ABERRATION

by

Shu-i Wang

A Thesis Submitted to the Faculty of the

COMMITTEE ON OPTICAL SCIENCES (GRADUATE)

In Partial Fulfillment of the Requirements
For the Degree of

MASTER OF SCIENCE

In the Graduate College

THE UNIVERSITY OF ARIZONA

1989

STATEMENT BY AUTHOR

This thesis has been submitted in partial fulfillment of requirements for an advanced degree at The University of Arizona and is deposited in the University Library to be made available to borrowers under rules of the Library.

Brief quotations from this thesis are allowable without special permission, provided that accurate acknowledgment of source is made. Requests for permission for extended quotation from or reproduction of this manuscript in whole or in part may be granted by the head of the major department or the Dean of the Graduate College when in his or her judgment the proposed use of the material is in the interests of scholarship. In all other instances, however, permission must be obtained from the author.

SIGNED: 

APPROVAL BY THESIS DIRECTOR

This thesis has been approved on the date shown below:

B. Roy Frieden
B. Roy Frieden
Professor of Optical Sciences

4/19/89
Date

ACKNOWLEDGEMENTS

I would like to thank Hughes Aircraft Company for providing the financial support for my Master of Science degree. I thank Dr. B. Roy Frieden who suggested this thesis topic and whose timely guidance and direction enabled me to complete this work. I also thank Dr. Lawrence and Dr. Shoemaker for consenting to be on my examination committee. Futhermore, I very much appreciate Dr. Shack's helpful discussion and patience.

Special thanks to the people at OSC who made me smile and provided me with invaluable moral support throughout my time in Tucson. I especially thank my 5th and 4th floor cubiclemates. I also thank Yiping Hu for our many discussions.

To my family, I wish to express my love and appreciation of their support and encouragement. I thank Michael Lee for making me laugh throughout difficult times, and his mom for relating his latest baby antics. And Shu Ming, for being a big sister. Most of all, I thank my parents, Po-Tsen Wang and Helen Yee Wang, for giving up their careers for their daughters.

To Jim Annis, I owe a special debt of gratitude (which I have no doubt he will make me pay back during the writing of his dissertation). Thank you for your love and support. You brought me happiness on a big scale.

This thesis is dedicated to my parents and James T. Annis.

TABLE OF CONTENTS

LIST OF FIGURES

Page

ABSTRACT

We derive the expression for the three-dimensional incoherent optical transfer function when third-order spherical aberration is present. The normalized version of the transfer function is numerically calculated for various amounts of spherical aberration. We find the effects of the aberration to be highly dependent on the spatial frequency in the longitudinal direction. We also calculate a structure content parameter, as a quality criterion, from the normalized transfer function. Remarkably, the structure content parameter dependence on spherical aberration is well-fit by a simple Cauchy curve for aberrations out to two waves at the margin.

I. INTRODUCTION

The field of two-dimensional Fourier optics is highly developed and has enjoyed wide applications. The natural extension of the theory into three-dimensions has been performed by several people. For example, Frieden[1] has derived the incoherent three-dimensional optical transfer function, Wolf[2] performed the theory for coherently trans-illuminated objects, and Streibl[3] extended the theory to partially coherent light. Wide use of the three-dimensional theory has been hindered by the limited bandpass region of the optical transfer function (referred to as the missing cone of spatial frequencies in much of literature) and by the lack of development of 3-D imaging systems.

Important applications of three-dimensional transfer theory in areas such as robotic vision, image restoration, medical optics, microscopy and material processing, however, has brought on recent interest in the field. For example, optical serial sectioning is often used in microscopy to observe the three-dimensional structure of a microscopic specimen. The technique involves examination of a series of two-dimensional images with different parts of the object in focus. Digital restoration of a 3-D object from a set of 2-D images and the corresponding 2-D transfer functions has been done by, for example, Agard[4]. The goal is to know the amount of 3-D information contained in a 3-D image distribution. Three-dimensional transfer theory describes the limitations an imaging system has in forming a three-dimensional image. Knowledge of a system's optical transfer function also enables us to reconstruct the image by devising an optimal filter to compensate for frequency degradation within the system passband. Hu and Frieden[5] have developed a method for restoration of longitudinal images, with the exten-

sion to three-dimensional images in progress. Innovative developments of three-dimensional imaging systems such as the one by Davies, McCormic and Yang[6] of a single exposure optical system for producing three-dimensional images with continuous parallax and no flipping or cardboarding are promising.

Although much work has been published in calculating the diffraction-limited three-dimensional optical transfer function, there is a lack of literature on the effects of aberration on it. (For calculations of the aberration-free three-dimensional optical transfer function and point spread function for different pupils, see for example Frieden[1] and Streibl[7].) The purpose of this thesis is to find the effects of third-order spherical aberration on the three-dimensional incoherent optical transfer function.

In this thesis, we apply Frieden's transfer theory for the three-dimensional object and include a third-order spherical aberration term. In his development, the required conditions of stationarity and superposition are specified. We assume that these conditions are met by the system considered in our development; that is, we assume the object to be isotomous and incoherent. If an object is not isotomic over its entire volume, it is to be divided into isotomous volumes such that the point spread function for each volume is invariant with respect to change in position of the Gauss point.

In Section II Part A of the thesis, we derive the three-dimensional incoherent optical transfer function with third-order spherical aberration, using Frieden's transfer theory. We also identify a normalized transfer function that is solely a function of the amount of aberration present and is independent of all other system parameters. In Part B, we numerically calculate the normalized transfer function and discuss the results.

In Section III, we consider a merit function to quantify the effect of the aberration on the transfer function. The structure content in the normalized transfer function is utilized as a quality criterion. We also curve-fit the plot of structure content versus spherical aberration.

II. OPTICAL TRANSFER FUNCTION

We derive and calculate numerically the three-dimensional incoherent optical transfer function with third-order spherical aberration.

A. Derivation

The notation used in this paper is identified in Figures 1 and 2. H and H′ are the principal points. The effective focal length of the system is f. Object and image distances are expressed in vector notation as

$$\mathbf{r}' = (x', y', z')$$

$$\mathbf{r}_G = (x_G, y_G, z_G)$$

and

$$\mathbf{r} = (x, y, z),$$

where $\mathbf{r}'$ is a general object point, $\mathbf{r}_G$ is the corresponding Gauss point, and $\mathbf{r}$ is a general point in the image space. In Figure 2, axes $\alpha'\beta'\gamma'$ have their origin at the Gauss point G. Axis γ' lies along the direction of $\mathbf{r}_G$, and axis α' lies in the plane that intersects $\mathbf{r}_G$ and the optical axis. Axes PQ are parallel to axes $\beta'\alpha'$. We assume field angles $\frac{(x_G^2+y_G^2)^{0.5}}{z_G}$ and $\frac{(x^2+y^2)^{0.5}}{z}$ to be small so that (α',β',γ') corresponds to (α,β,γ) where (α,β,γ) is the coordinate system for a general image point. In other words, the paraxial approximation is assumed. The reference sphere in Figure 2 has radius r_G and intersects the optical axis at H′. The wave aberration used later in the development is the deviation of the actual wavefront from the reference sphere.

Using the above notation, Frieden's paper derived the "complete" optical transfer function $F(\Omega)$ for three-dimensional image formation as

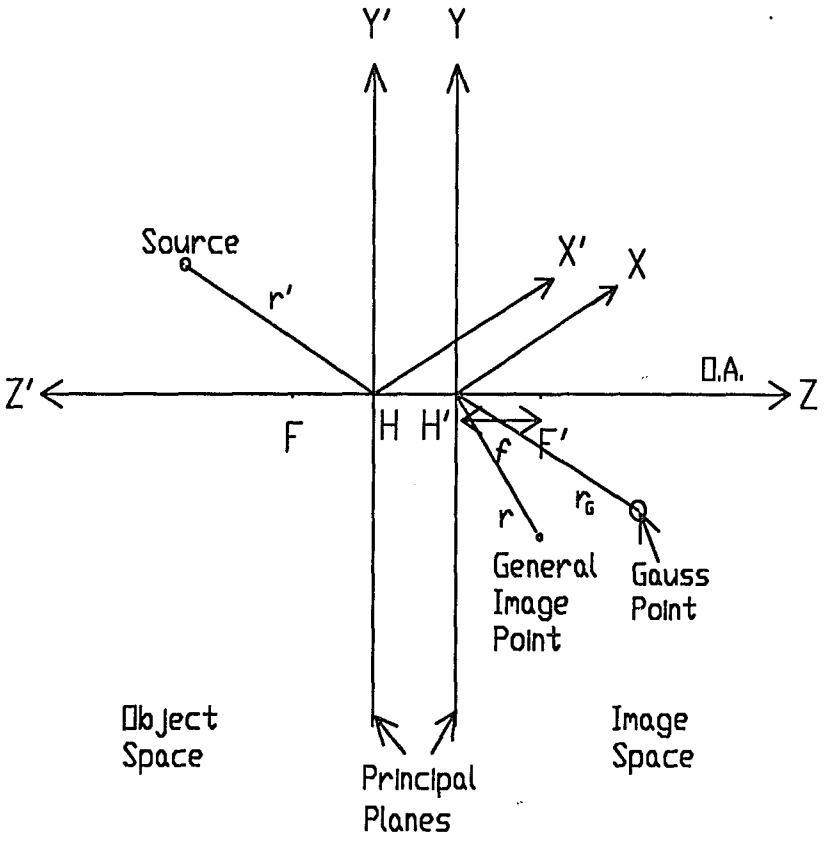

Figure 1. Parameters of the object and image space for three-dimensional image formation.

$$F(\Omega) = \frac{r_G}{\sqrt{2\pi}|\omega_1|}\int_{-\infty}^{\infty} dq U(p(q), q) U^* \left[p(q) - \frac{r_G\omega_1}{\kappa}, q - \frac{r_G\omega_2}{\kappa}\right] \quad (1)$$

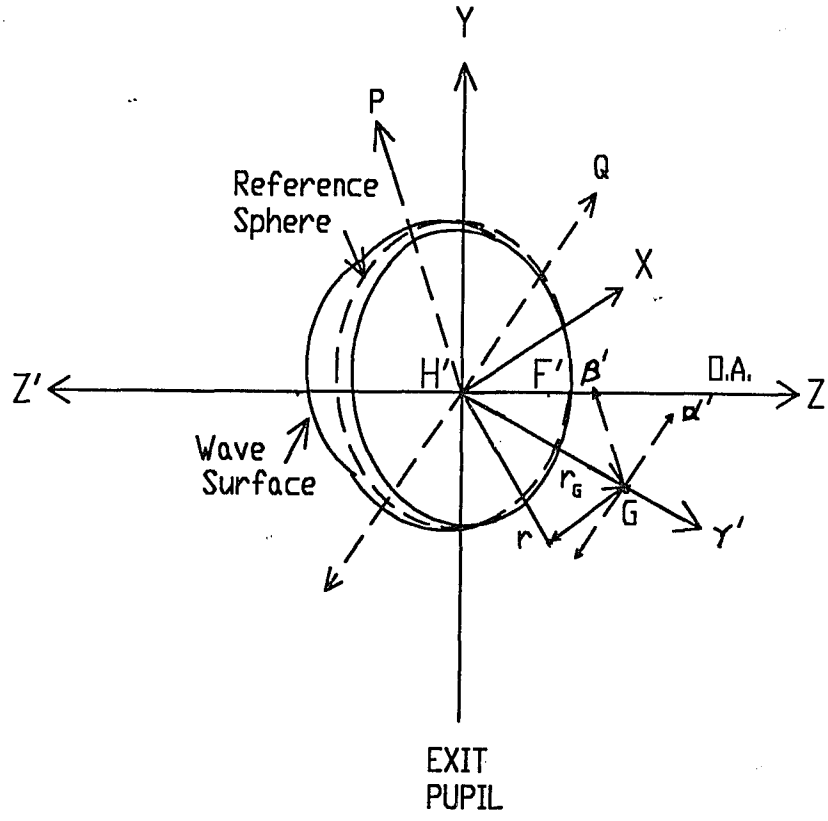

Figure 2. Parameters of the pupil and spread function space.

where

$$\bar{p}(q) = \frac{r_G \frac{\omega^2}{2\kappa} + r_G \omega_3 - q\omega_2}{\omega_1}. \qquad (2)$$

In Equations (1) and (2), $(\omega_1, \omega_2, \omega_3) = \Omega$ are the spatial frequencies, $\omega = (\omega_1, \omega_2)$, and

U(p, q) is the generalized pupil function,

$$U(p,q) = U_o(p,q)e^{j\kappa W}$$

U_o = diffraction-limited pupil function,

W = wave aberration function.

Note that because of the dependence p(q), the integral (1) is actually a line integral. The line lies within the overlap (autocorrelation) region of the pupil U and its displaced conjugate U^*.

For third-order spherical aberration,

$$W = W'_{040}\rho^4$$

where

ρ = pupil coordinate

$$= \sqrt{p^2+q^2}$$

and

$$W'_{040} = \frac{W_{040}}{Y_E^4}$$

W_{040} = spherical aberration coefficient

Y_E = pupil height.

Therefore, $F(\Omega)$ for the case of third-order spherical aberration is

$$F(\Omega) = \frac{r_G}{\sqrt{2\pi}|\omega_1|}\int_{-\infty}^{\infty} dq U_o(p(q),q)U_o^*\left[p(q)-\frac{r_G\omega_1}{\kappa}, q-\frac{r_G\omega_2}{\kappa}\right]$$

$$\times e^{j\kappa W'_{040}\left[(p(q)^2+q^2)^2-\left[\left[p(q)-\frac{r_G\omega_1}{\kappa}\right]^2+\left[q-\frac{r_G\omega_2}{\kappa}\right]^2\right]^2\right]}. \qquad (3)$$

Referring to Figure 3, the line integral in (3) may be simplified by replacing the integration variable q by a coordinate l along the integration path such that

$$q = \frac{\omega_1}{\omega} l + r_G \frac{\omega_2}{2\kappa} + r_G \omega_2 \frac{\omega_3}{\omega^2} \tag{4}$$

$$dq = \frac{\omega_1}{\omega} dl \tag{5}$$

and

$$p = -\frac{\omega_2}{\omega} l + r_G \frac{\omega_1}{2\kappa} + r_G \omega_1 \frac{\omega_3}{\omega^2}. \tag{6}$$

Integration path l is located at a distance of $b(\Omega)$ from origin O, perpendicular to (OO'), where

$$b(\Omega) = r_G \frac{\omega}{2\kappa} + r_G \frac{\omega_3}{\omega}. \tag{7}$$

Note that at $\omega_3=0$, $b(\Omega)=\frac{OO'}{2}$, and integration path l becomes the perpendicular bisector of (OO'). The pupils are then symmetric about path l.

Combining (4) and (6), the quartic p and q terms in the exponent of (3) reduce to a quadratic term in l:

$$[p^2+q^2]^2 - \left[\left[p - \frac{r_G \omega_1}{\kappa}\right]^2 + \left[q - \frac{r_G \omega_2}{\kappa}\right]^2\right]^2$$

$$= \left[4 r_G{}^2 \frac{\omega_3}{\kappa}\right]\left[l^2 + \left[r_G \frac{\omega_3}{\omega}\right]^2 + \left[r_G \frac{\omega}{2\kappa}\right]^2\right]. \tag{8}$$

By substitution of (4)-(6) into (3),

$$F(\Omega) = \frac{r_G}{\sqrt{2\pi}\omega} \int_{A'}^{A} dl U_o(l) U_o^*(l') \, e^{j4W'_{040} r_G{}^2 \omega_3 \left[l^2 + \left[r_G \frac{\omega_3}{\omega}\right]^2 + (r_G \frac{\omega}{2\kappa})^2\right]}. \tag{9}$$

Endpoints A and A' are determined by the overlap region of U and U*. For a circular clear pupil with only third-order spherical aberration present, we have

$$U_o(l) U_o^*(l') = 1$$

along the integration path, and

$$A = -A' = \sqrt{Y_E{}^2 - \left[r_G \frac{\omega}{2\kappa} + r_G \frac{|\omega_3|}{\omega}\right]^2}. \tag{10}$$

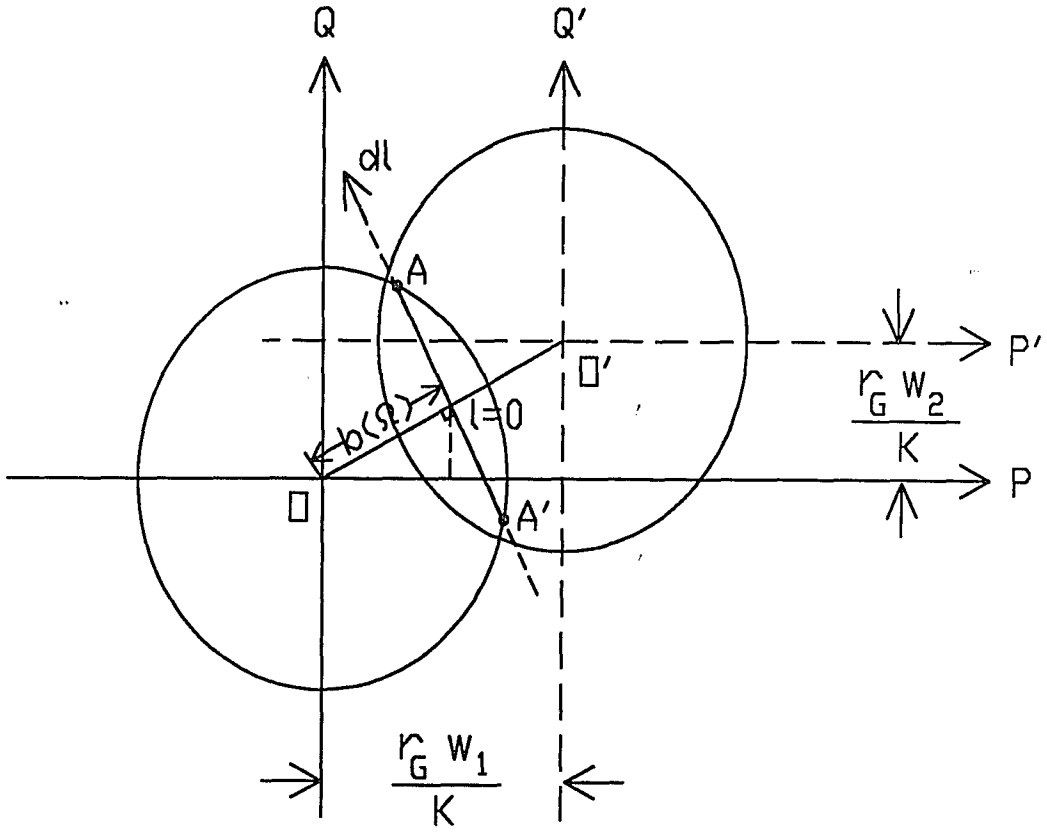

Figure 3. Line integral *dl* for optical transfer function F(Ω).

Hence,

$$F(\Omega) = \frac{2r_G}{\sqrt{2\pi}\omega} \int_0^A dl\, e^{j4W'_{040} r_G^2 \omega_3 \left[l^2 + \left[r_G \frac{\omega_3}{\omega} \right]^2 + (r_G \frac{\omega}{2\kappa})^2 \right]}. \qquad (11)$$

Equation (11) shows that the amplitude and phase of the optical transfer function

depends on the image distance, wavelength of light, pupil height, and amount of aberration at the edge of the pupil. At ω_3=0, Equation (11) becomes

$$F(\omega_1,\omega_2,0) = \frac{2r_G}{\sqrt{2\pi}\omega}\sqrt{Y_E^2-\left[r_G\frac{\omega}{2\kappa}\right]^2}\ , \tag{12}$$

and the transfer function reduces to the diffraction-limited case. Equation (12) shows that $F(\omega_1,\omega_2,0)$ is a real function, independent of spherical aberration. Another way to visualize this result is by referring to Figure (3): the two conjugate displaced pupils are symmetric about the integration path when ω_3=0; for even aberrations, the phase contributions from the two pupils cancel and the aberrations (which give rise to the phase terms) have no effect. As in the diffraction-limited case, $F(\Omega)$ has a simple pole at ω=0.

To facilitate the practical use of the transfer function, we define, as in Frieden's paper, a normalized transfer function $\mathcal{F}(\Omega)$ proportional to $F(\Omega)$:

$$\mathcal{F}(\Omega) = \sqrt{2\pi}\frac{\omega}{r_G}\ \frac{F(\Omega)}{\int_{-\infty}^{\infty}|U(\rho,\theta)|^2\,d\rho} \tag{13}$$

where

$$\theta = \tan^{-1}\left[\frac{\omega_1}{\omega_2}\right]. \tag{14}$$

$\mathcal{F}(\Omega)$ has the following advantageous properties: (1) it has only one parameter -- the amount of aberration at the edge of the pupil in units of wavelength, (2) it is unitless, and (3) it is bounded at all ω.

To express $\mathcal{F}(\Omega)$, we first calculate the normalization integral in the denominator of (13). For a circular unvignetted pupil,

$$\int_{-\infty}^{\infty}|U(\rho,\theta)|^2\,d\rho = \int_{-Y_E}^{Y_E}d\rho = 2Y_E. \tag{15}$$

Substitution of (11) and (15) into (13) yields

$$\mathcal{F}(\Omega) = \frac{1}{Y_E}\int_0^A dl\, e^{j4W'_{040}r_G^2\omega_3\left[l^2+\left[r_G\frac{\omega_3}{\omega}\right]^2+(r_G\frac{\omega}{2\kappa})^2\right]}. \quad (16)$$

Properties (1) and (2) are accomplished by expressing ω and ω_3 in terms of their cutoff frequencies. The bandpass region for F (or $\mathcal{F}$) was derived in Frieden's paper. The cutoff frequencies for ω and ω_3 are respectively

$$\omega_c = \frac{4\pi Y_E}{\lambda|r_G|}. \quad (17)$$

$$\omega_{3c} = \frac{\pi Y_E^2}{\lambda r_G^2}. \quad (18)$$

Note, $\omega_{3c}=\frac{NA}{4}\omega_c$ where $NA=\frac{Y_E}{r_G}$. Therefore, the cutoff in the longitudinal frequency component is limited by the numerical aperture. Physically, the finite support in the spatial frequency domain is caused by the finite core of light accepted by the system aperture and by diffraction. See Figure 4. Macias-Garza, Bovik, and Diller[8] showed that as the aperture is increased, both the 3-D bandpass region and the low-pass distortion of the spatial frequencies improve.

We define normalized frequencies ω_n and ω_{3n} as

$$\omega_n = \frac{\omega}{\omega_c}, \quad (19)$$

$$\omega_{3n} = \frac{\omega_3}{\omega_{3c}}. \quad (20)$$

In terms of the original frequencies,

$$\omega = \frac{4\pi Y_E}{\lambda|r_G|}\omega_n, \quad (21)$$

$$\omega_3 = \frac{\pi Y_E^2}{\lambda r_G^2}\omega_{3n}. \quad (22)$$

Furthermore, let

$$l' = \frac{l}{Y_E}, \quad (23)$$

$$dl = Y_E dl'. \quad (24)$$

Applying the change of variables defined in (21)-(24) to Equations (16) and (10), we obtain

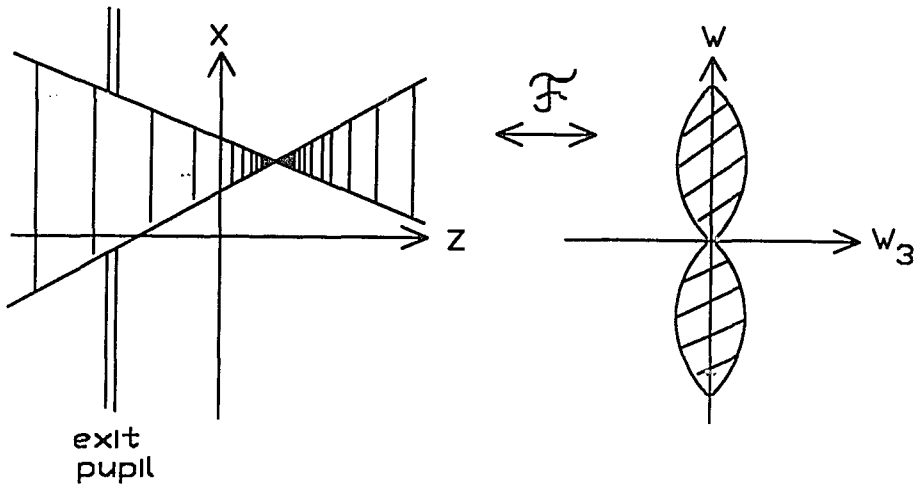

Light cone emerging from a finite aperture Bandpass region of the 3-D OTF

Figure 4. Relationship between numerical aperture and bandpass region.

$$\mathcal{F}(\Omega) = \int_0^{A''} dl' \, e^{j2\kappa W'_{040}\omega_{3n}\left[l'^2+\left[\frac{\omega_{3n}}{4\omega_n}\right]^2+\omega_n{}^2\right]}, \tag{25}$$

$$A'' = \sqrt{1-\left[\omega_n+\frac{\omega_{3n}}{4\omega_n}\right]^2}. \tag{26}$$

Expressing the spherical aberration coefficient in units of wavelength

$$W_{040} = a\lambda \tag{27}$$

results in the form of $\mathcal{F}$ which satisfies Properties (1-3):

$$\mathcal{F}(\Omega) = \int_0^{A''} dl' \, e^{j4\pi a\omega_{3n}\left[l'^2 + \left[\frac{\omega_{3n}}{4\omega_n}\right]^2 + \omega_n^2\right]}. \tag{28}$$

An important application of $\mathcal{F}(\Omega)$ is in calculating the image distribution. From Fourier theory,

$$i(x,y,z) = \frac{1}{(2\pi)^{\frac{3}{2}}} \iiint d\omega_1 \, d\omega_2 \, d\omega_3 O(\omega_1,\omega_2,\omega_3) F(\omega_1,\omega_2,\omega_3) e^{j(\omega_1 x+\omega_2 y+\omega_3 z)} \tag{29}$$

or, for rotationally symmetrical systems,

$$i(\xi,z) = \frac{1}{\sqrt{2\pi}} \int d\omega_3 e^{j\omega_3 z} \int d\omega O(\omega,\omega_3)\omega F(\omega,\omega_3) J_o(\xi\omega) \tag{30}$$

where

$$\xi = \sqrt{x^2+y^2}. \tag{31}$$

Combining Equations (13) and (15), we obtain

$$F(\omega,\omega_3) = 2Y_E \frac{r_G}{\sqrt{2\pi\omega}} \mathcal{F}(\omega,\omega_3). \tag{32}$$

Substitution of (32) into (30) yields

$$i(\xi,z) = Y_E \frac{r_G}{\pi} \int d\omega_3 e^{j\omega_3 z} \int d\omega O(\omega,\omega_3) \mathcal{F}(\omega,\omega_3) J_o(\xi\omega). \tag{33}$$

Thus, $\mathcal{F}$ and not F is the transfer function used in Fourier theory applications. This solves the problem of the singularity contained in F at Ω=0.

B. Calculation and Discussion

Equation (28) was numerically calculated for the following amounts of third-order spherical aberration: 0, 0.25λ, 0.5λ, 0.75λ, λ, 1.5λ, 2λ, 2.5λ, and 3λ. The computer program used to calculate Equation (28), FSCRIPT.FOR, is presented in Appendix A. Program FSCRIPT.FOR is written in VAX FORTRAN and calls on a numerical integration subroutine which uses quadrature formulae developed at the Jet Propulsion Laboratory[9,10]. The integration subroutine outputs the estimated integration error along with

the data. The estimated error in the $\mathcal{F}$ calculations is about 0.1 percent, well within the accuracy of the plotter. When the integration is performed with twice the number of subdivisions, the numerical results are within 0.05 percent. Also, since $\mathcal{F}$ is the sum of two Fresnel integrals[11], we verified by hand random values of $\mathcal{F}(\Omega, W_{040})$, using the tabulated values of the Fresnel integrals in Reference 11. The hand calculated values are within 0.01 percent of the numerically integrated values.

The data generated from the program are presented in Figures 4-20 in the form of surface plots. Figures 5-13 display the magnitude, M, of $\mathcal{F}$. The magnitude of $\mathcal{F}$ is greatest at ω_3=0; this is reasonable since then the aberration term vanishes in Equation (28). A comparison of the magnitude surface plots in Figures 5 and 6 shows that there is little change between the diffraction-limited case and the quarter-wave aberrated case, confirming Rayleigh's quarter-wave rule. A significant change in the magnitude of $\mathcal{F}$ starts to appear at $W_{040}=\lambda$, and develops into a larger oscillatory region with increasing amounts of aberration. The change in the magnitude of $\mathcal{F}$ is analogous to the two-dimensional optical transfer function's behavior with spherical aberration. (For reference on the two-dimensional case, see for example Barakat and Houston[12].) Note, however, that the spherical aberration causes low-pass attenuation in the direction of ω_3, and has no effect when ω_3=0 (as discussed in section A). For example, when W_{040}=0 and the magnitude M of $\mathcal{F}$ is fixed at 0.7, the maximum ω_{3n} is approximately 0.51, and the maximum ω_n is 0.71. When W_{040}=0.25λ and M=0.7, the maximum ω_{3n} drops to 0.48, but the maximum ω_n stays at 0.71. (See Figures 5 and 6.)

Unlike the magnitude, the phase transfer function for the three-dimensional case is very different from the two-dimensional case. In two-dimensions, the optical transfer function (OTF) in the presence of symmetrical aberrations (such as spherical aberration) is a real function. However, we may consider the OTF to have a phase component which undergoes a π change whenever the OTF changes sign. For example, the phase

of the OTF is zero at ω=0, jumps to π when the OTF changes sign, and remains π until the OTF changes sign again. By contrast, for the three-dimensional case, the phase term P of $\mathcal{F}$ changes *continuously* with frequency, as shown in Figures 14-21. Phase P does not exhibit the abrupt phase changes that its 2-D counterpart does. The phase is plotted as a function of the transverse and longitudinal frequencies, from dc to cutoff. Although not plotted, Equation (28) shows that $P(\omega_3<0)=-P(|\omega_3|)$. (There is no phase term for the diffraction-limited case, of course). The phase shift is zero at ω_3=0, and increases monotonically with ω_3. This is because the longitudinal frequency ω_3 causes the integration path to deviate from the line of symmetry between the two displaced pupils, thereby causing a phase change. (See Figure 3.)

An interesting phase effect may be noted: the maximum phase change occurs at the cutoff condition (ω=0.5ω_c,ω_3=ω_{3c}). The amount of this maximum phase change is exactly equal to W_{040}, the amount of third order spherical aberration at the edge of the pupil. For example, the maximum phase change is 2π for one wave of aberration. This may be explained as follows.

To derive the maximum phase change condition, we recall that P increases monotonically with ω_3. Therefore, the maximum phase should occur at the cutoff frequency ω_{3c}. This corresponds to ω_{3n}=1. From Equation (26), we need

$$\omega_n + \frac{\omega_{3n}}{4\omega_n} \leq 1. \tag{34}$$

At ω_{3n}=1, (34) becomes

$$\omega_n + \frac{1}{4\omega_n} \leq 1. \tag{35}$$

The only solution for (35) is ω_n=0.5. Therefore, the maximum phase change occurs at (ω_n=0.5,ω_{3n}=1), equivalent to (ω=0.5ω_c,ω_3=ω_{3c}). Note that the maximum phase change occurs at a cutoff point, and $\mathcal{F}\equiv$0 at cutoff. However, the maximum phase change rule still serves as a convenient phase measure since the phase of $\mathcal{F}$ will be everywhere less than the maximum phase of $2\pi a$ and approaches it as the frequencies approach

(ω=0.5ω_c, ω_3=ω_{3c}).

To find the maximum phase, we refer to Equation (28). Taking the limit as we approach the maximum phase point,

$$\mathcal{F}(\omega_n \to 0.5, \omega_{3n} \to 1) = \Delta\, e^{j4\pi a\omega_{3n}\left[\Delta^2 + \left[\frac{\omega_{3n}}{4\omega_n}\right]^2 + \omega_n{}^2\right]}, \tag{36}$$

where

$$\Delta = A'' = \sqrt{1 - \left[\omega_n + \frac{\omega_{3n}}{4\omega_n}\right]^2}. \tag{37}$$

The phase is then

$$P = 4\pi a\omega_{3n}\left[1 - \left[\omega_n + \frac{\omega_{3n}}{4\omega_n}\right]^2 + \left[\frac{\omega_{3n}}{4\omega_n}\right]^2 + \omega_n{}^2\right]$$

$$= 4\pi a\left[\omega_{3n} - \frac{\omega_{3n}{}^2}{2}\right]. \tag{38}$$

As $\omega_{3n} \to 1$,

$$P \to P_{max} = 2\pi a. \tag{39}$$

This agrees with the numerically calculated results.

To summarize, the magnitude of $\mathcal{F}$ exhibits oscillatory regions with greater than one wave of third-order spherical aberration present, much like the type of behavior in the two-dimensional magnitude transfer function with spherical aberration. $\mathcal{F}$ is independent of aberration at ω_3=0, and reduces to the diffraction-limited case. Unlike the two-dimensional case, $\mathcal{F}$ has a phase which varies continuously with frequency. This phase effect is due to the frequency in the longitudinal direction, ω_3, and it increases monotonically with ω_3. The phase of $\mathcal{F}$ approach the maximum of $2\pi a$ as the frequencies approach (ω=0.5ω_c, ω_3=ω_{3c}).

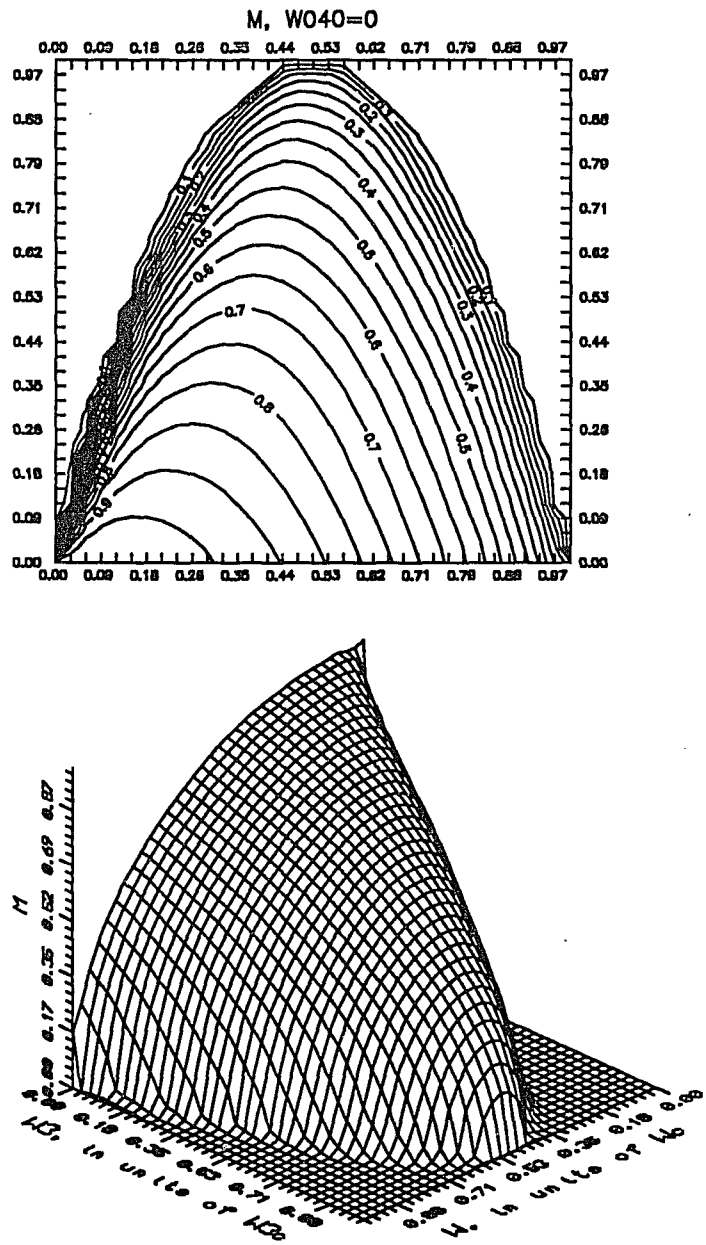

Figure 5. Magnitude of $\mathcal{F}$, diffraction-limited case.

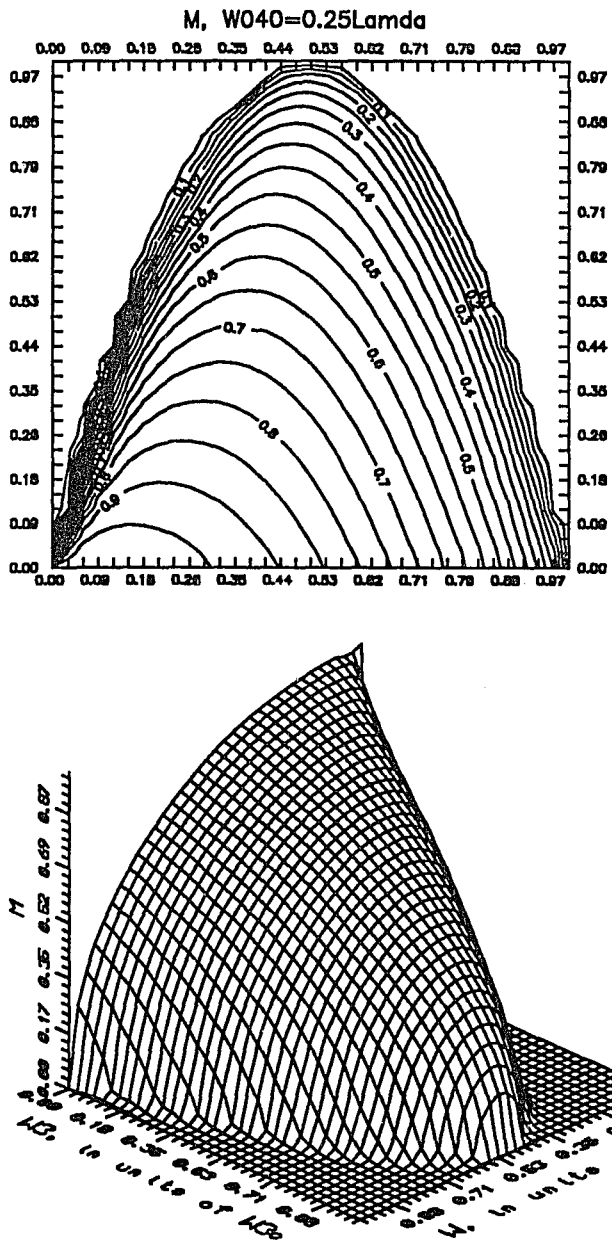

Figure 6. Magnitude of $\mathcal{F}$, W_{040}=0.25λ.

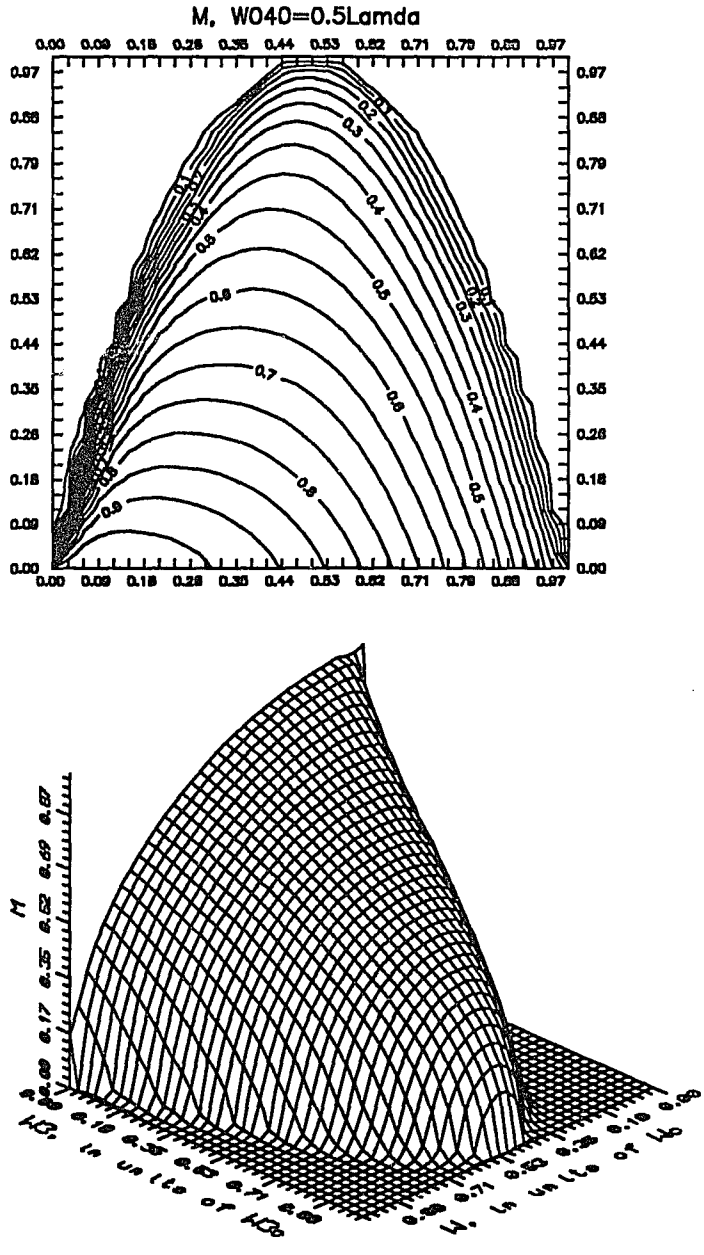

Figure 7. Magnitude of $\mathcal{F}$, $W_{040}=0.5\lambda$.

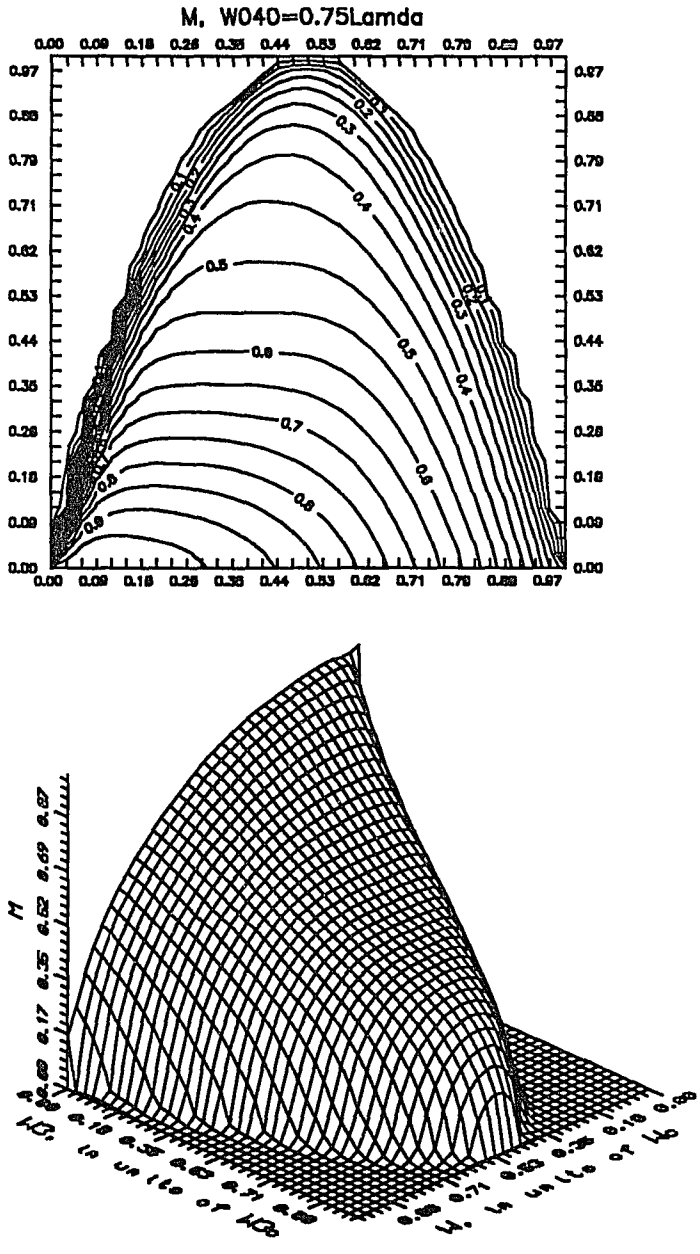

Figure 8. Magnitude of $\mathscr{F}$, W_{040}=0.75λ.

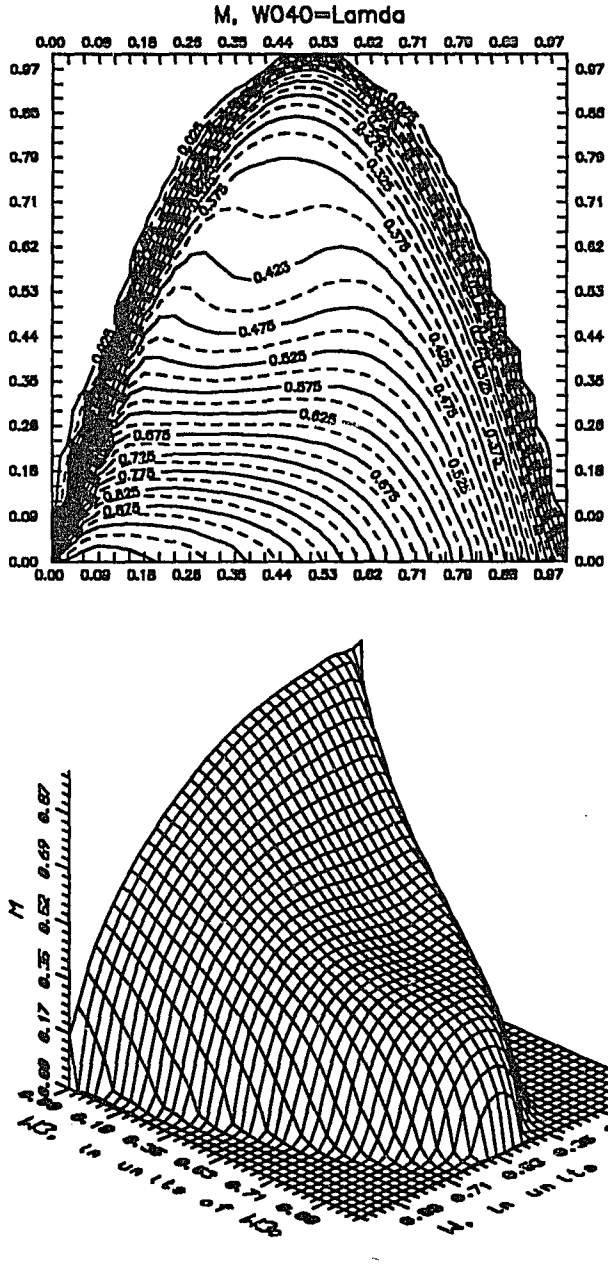

Figure 9. Magnitude of $\mathscr{F}$, $W_{040}=\lambda$.

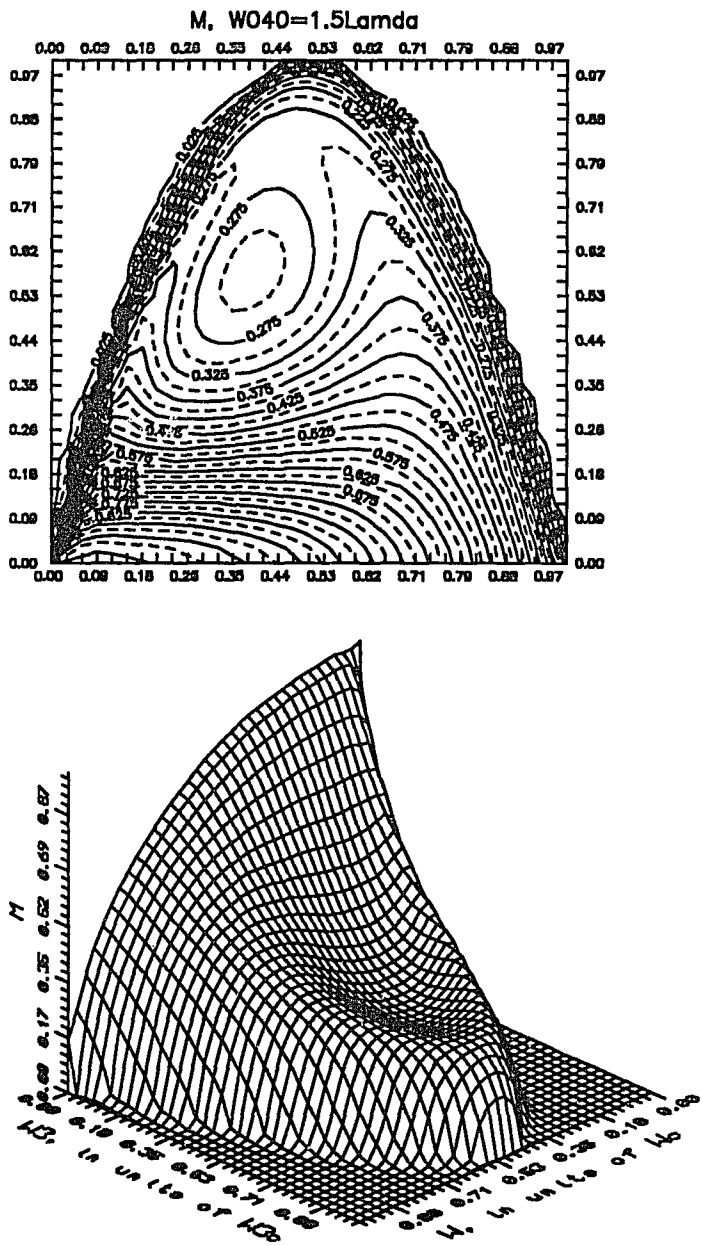

Figure 10. Magnitude of $\mathscr{F}$, $W_{040}=1.5\lambda$.

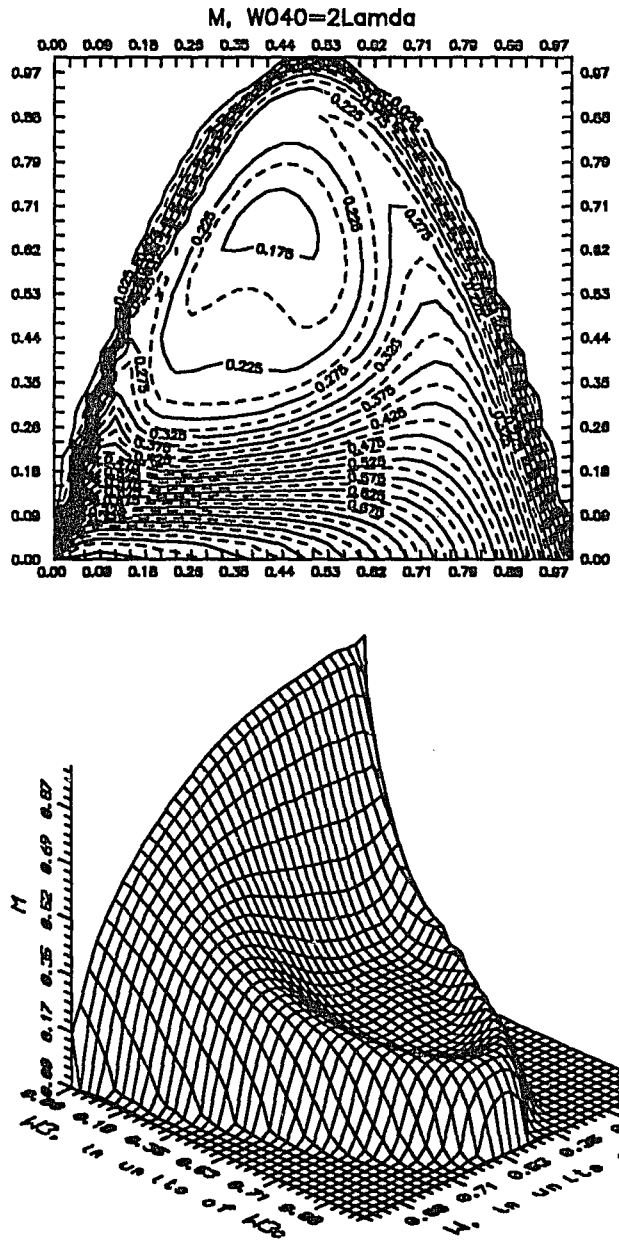

Figure 11. Magnitude of $\mathcal{F}$, $W_{040}=2\lambda$.

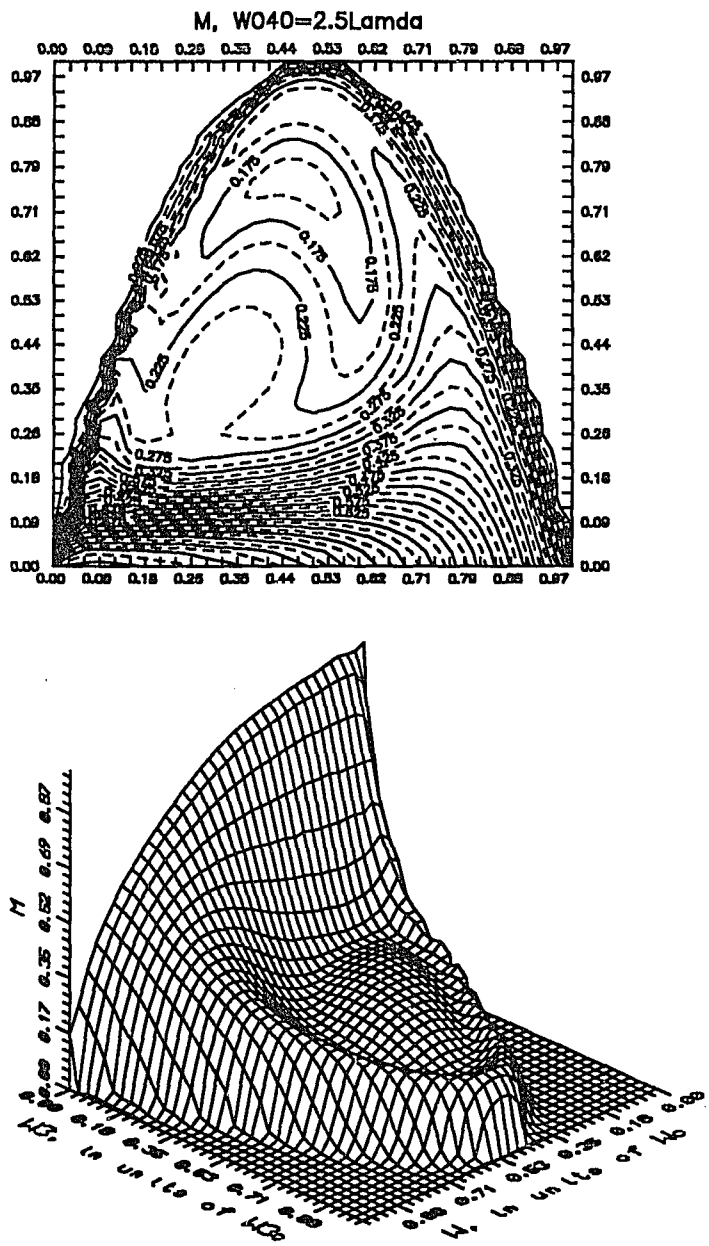

Figure 12. Magnitude of $\mathscr{F}$, W_{040}=2.5λ.

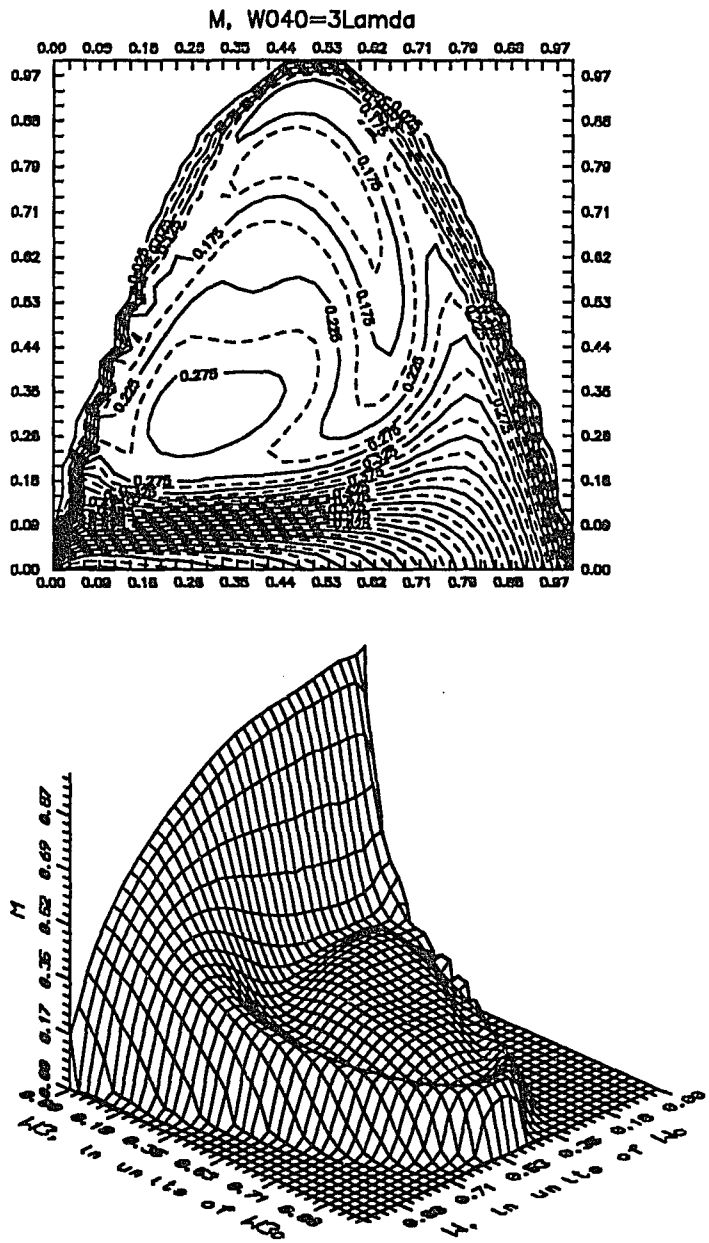

Figure 13. Magnitude of $\mathscr{F}$, $W_{040}=3\lambda$.

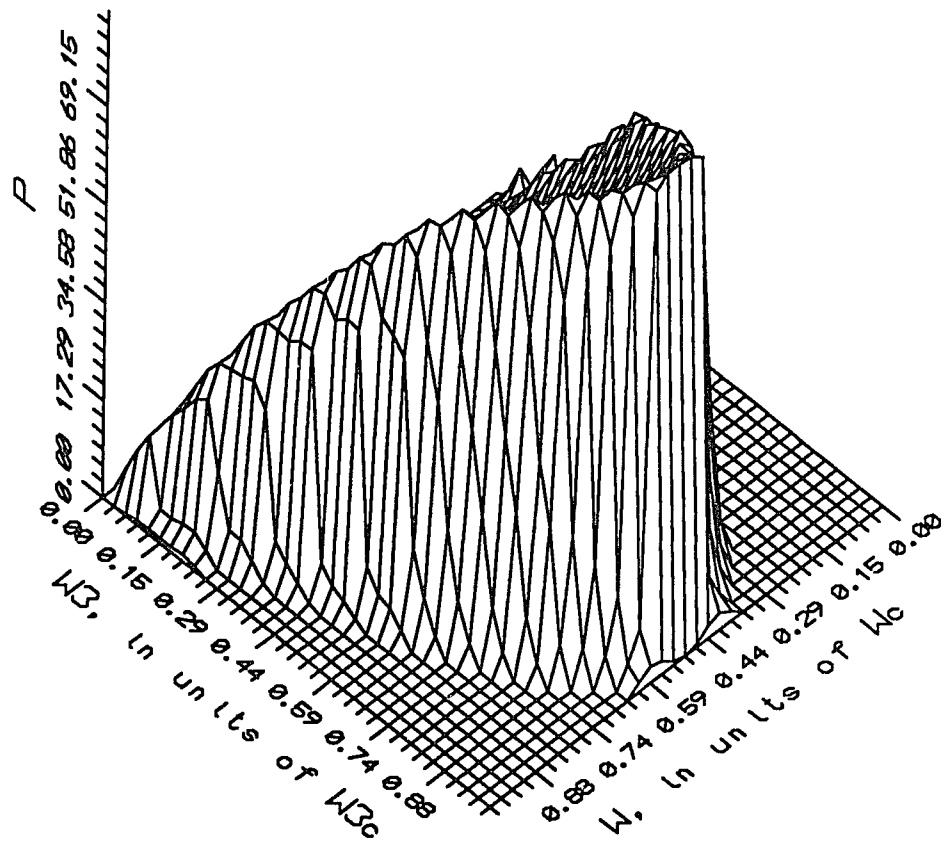

Figure 14. Phase of $\mathcal{F}$, W_{040}=0.25λ

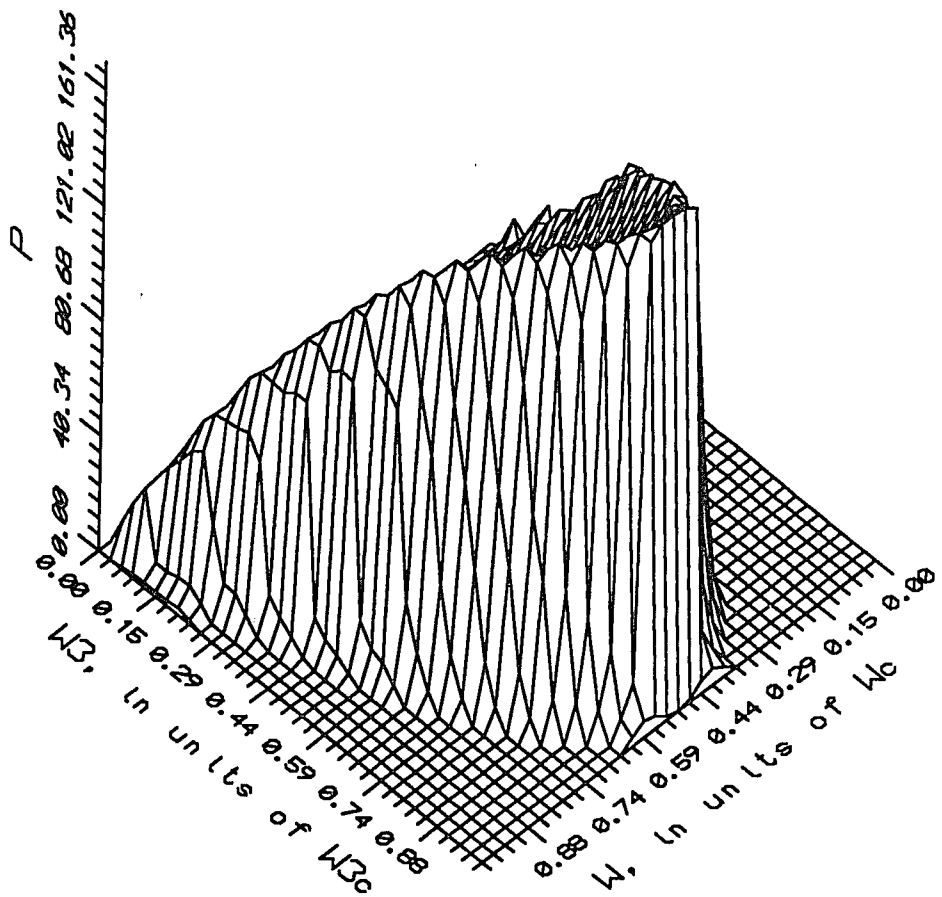

Figure 15. Phase of $\mathcal{F}$, $W_{040}=0.5\lambda$.

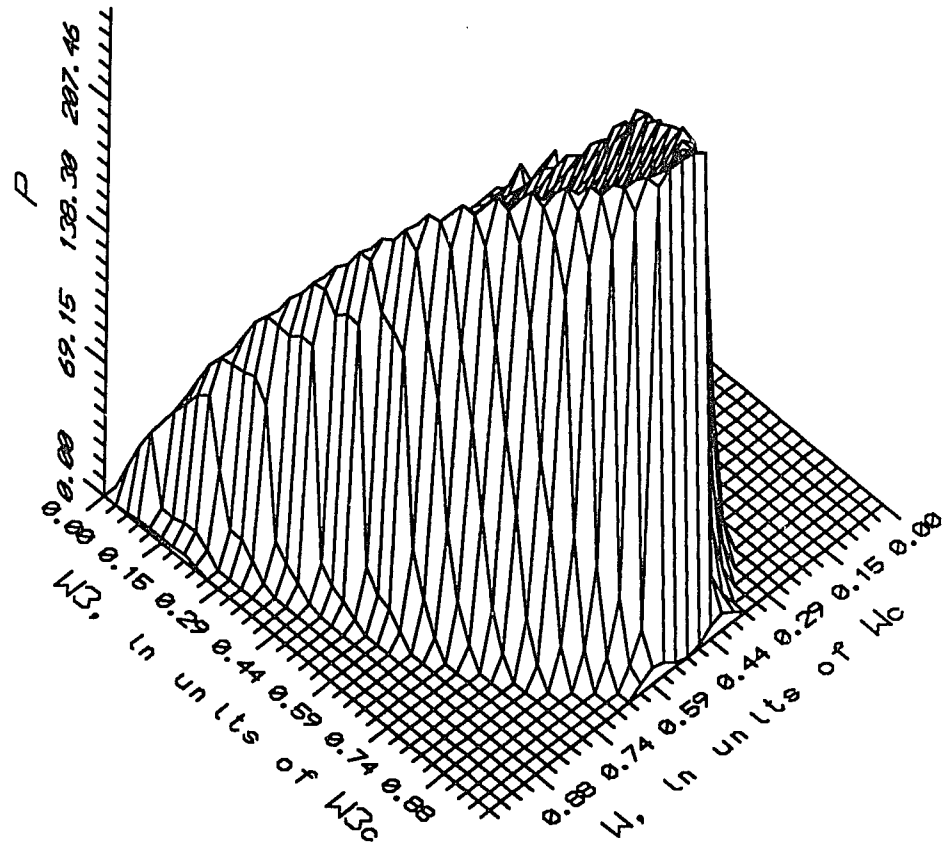

Figure 16. Phase of $\mathcal{F}$, W_{040}=0.75λ.

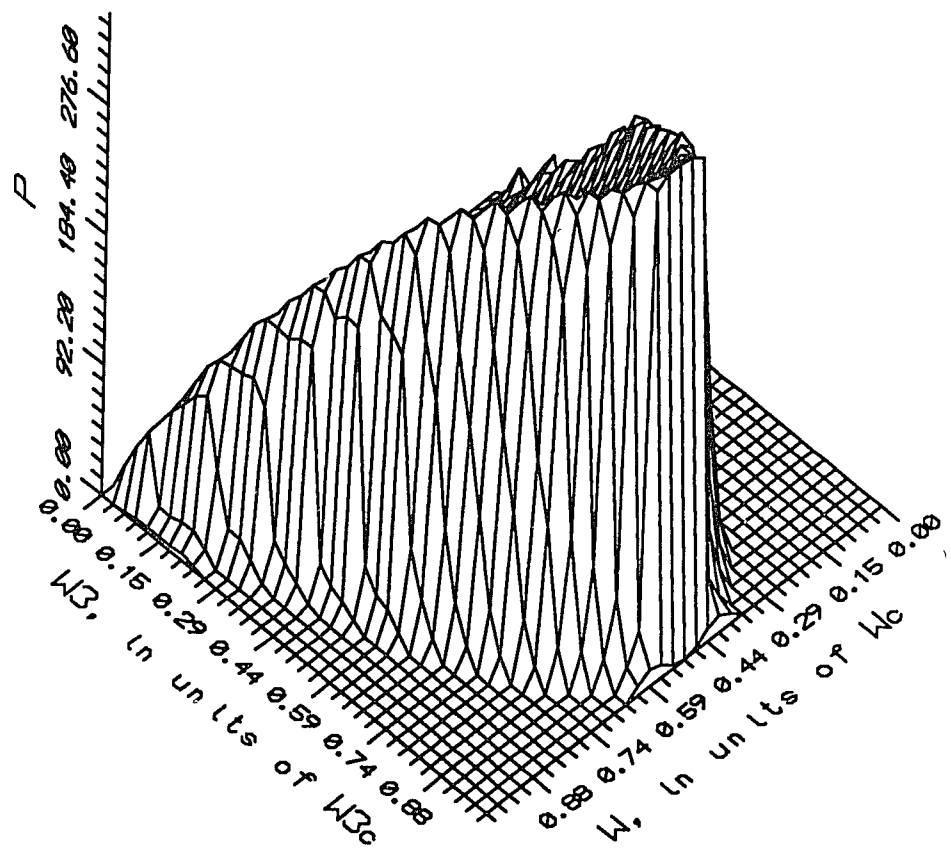

Figure 17. Phase of $\mathcal{F}$, $W_{040}=\lambda$.

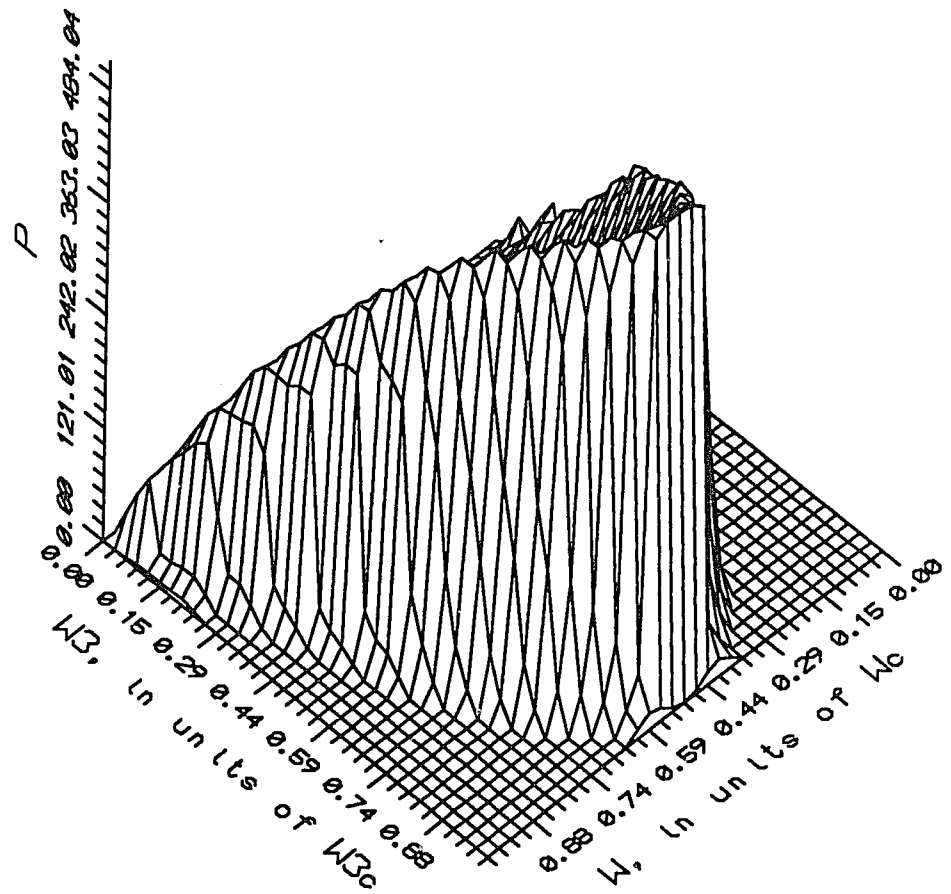

Figure 18. Phase of $\mathcal{F}$, W_{040}=1.5λ.

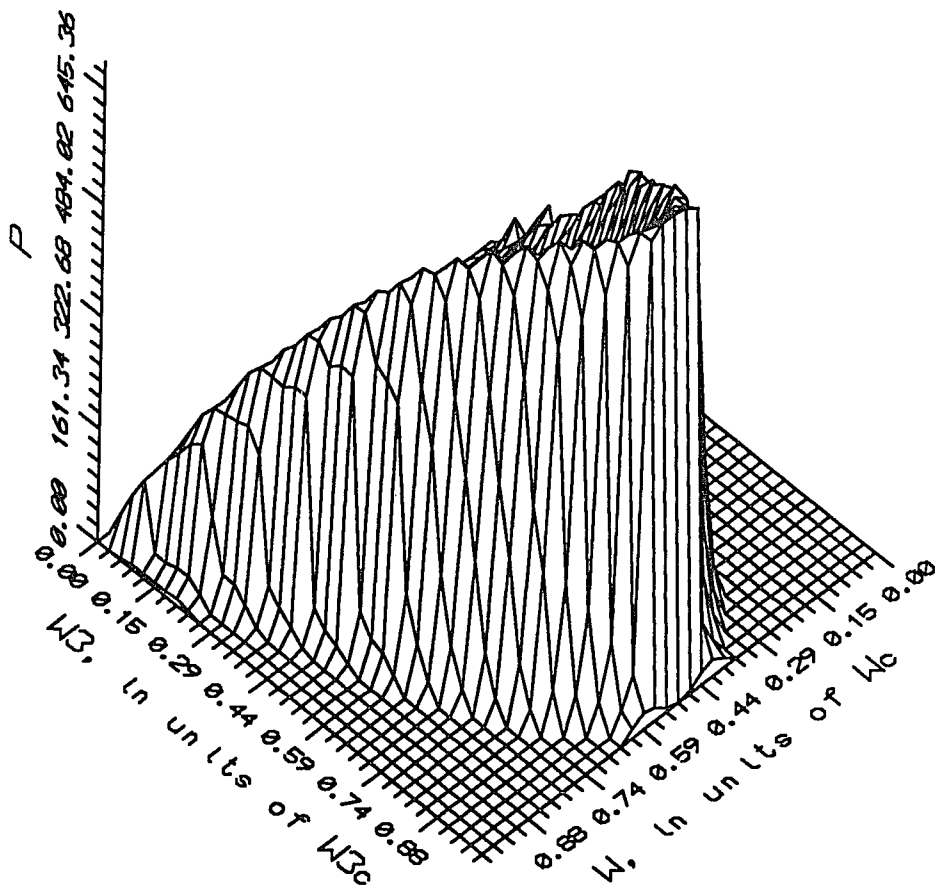

Figure 19. Phase of $\mathcal{F}$, $W_{040}=2\lambda$.

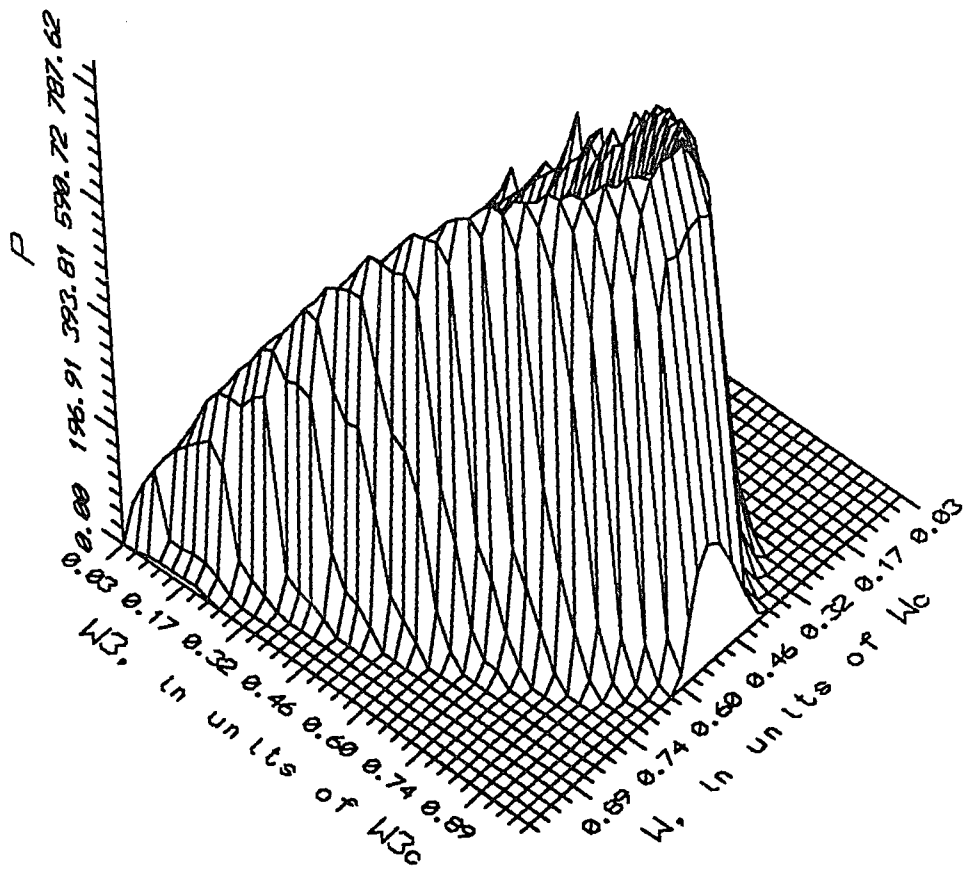

Figure 20. Phase of $\mathcal{F}$, W_{040}=2.5λ.

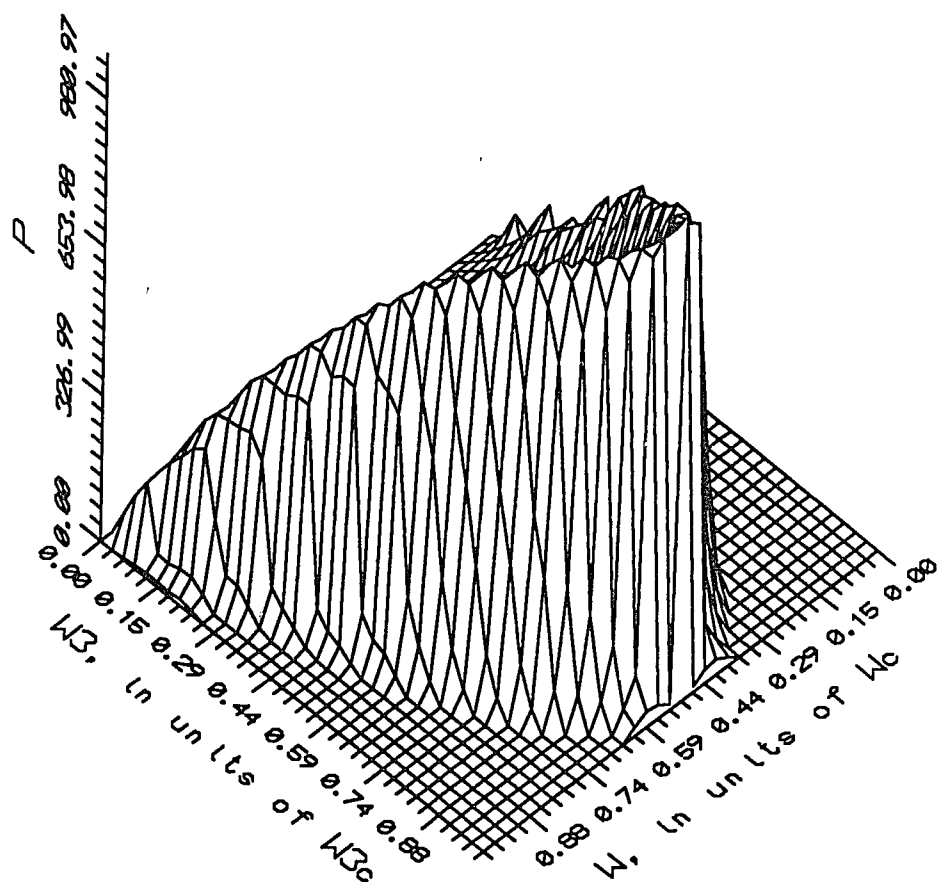

Figure 21. Phase of $\mathcal{F}$, $W_{040}=3\lambda$.

III. A FIGURE OF MERIT

We derive and calculate a quality criterion to quantify the effect of aberration on the three-dimensional incoherent optical transfer function. This is the "structural content" in the spread function.

Linfoot[13] described the quantity of structural content in the image as a measure of image quality. The structure content measures the capacity of the system to reproduce fine object details. It is defined as

$$T_i = \int_{\mathbf{r}} \mathrm{I}^2 \mathrm{d}\mathbf{r}, \tag{40}$$

where I is the image distribution. If the image distribution is gaussian, T_i is inversely proportional to the standard deviation, and therefore inversely measures the spread in the image. (The larger the spread, the larger the aberration present, the smaller T_i becomes, and the more degraded the high frequency components.)

Backus and Gilbert[14] defined a similar quantity as the structure content,

$$l_r^2 = \int_{\infty}^{\infty} x^2 f(x)^2 dx, \tag{41}$$

where l_r is the resolution length and f is the point spread function. However, for our purposes the conversion of the point spread function integral in (41) to the optical transfer function is not convenient, since the calculation of l_r involves the square of the *derivative* of the optical transfer function. We therefore choose to use the structure content (40) as the more convenient and direct merit function in describing the effect of aberration on the optical transfer function.

For a single object point radiator, the irradiance distribution at the image plane is given by the point spread function, $f(\mathbf{r}-\mathbf{r_G})$. On this basis, the three-dimensional structure content in the spread function would be

$$T_S = \int_{\mathbf{r}-\mathbf{r_G}} |f(\mathbf{r}-\mathbf{r_G})|^2 d(\mathbf{r}-\mathbf{r_G}). \tag{42}$$

From Parseval's theorem,

$$\int_{-\infty}^{\infty} |f(\alpha)|^2 d\alpha = \int_{-\infty}^{\infty} |F(\beta)|^2 d\beta, \tag{43}$$

where f and F are Fourier transform pairs. Therefore, another way to find T_S is to use the optical transfer function,

$$T_S = \int_{\Omega} |F(\Omega)|^2 d\Omega. \tag{44}$$

Unfortunately, quantity $|F(\Omega)|^2$ in (44) has a pole of order two at the origin, and is a function of the image distance and pupil height. Fortunately, the normalized transfer function $\mathscr{F}$ does not have a pole and is unitless. We therefore define the structure content in the transfer function using the normalized $\mathscr{F}$,

$$T_{Sn} = \int d\omega_n \int d\omega_{3n} |\mathscr{F}(\omega_n, \omega_{3n})|^2. \tag{45}$$

The diffraction-limited case of T_{Sn} is easily obtained by combining (26), (28) and (45),

$$\begin{aligned} T_{Sno} &= 2\int_0^1 d\omega_n \int_0^{4(\omega_n-\omega_n^2)} d\omega_{3n} \left[1-\left[\omega_n+\frac{\omega_{3n}}{4\omega_n}\right]^2\right] \\ &= 2\int_0^1 d\omega_n \left[\frac{8}{3}\omega_n - 4\omega_n^2 + \frac{4}{3}\omega_n^4\right] \\ &= 0.53333, \end{aligned} \tag{46}$$

a pure number.

Program NEWRES.FOR listed in Appendix B numerically calculates Equation (45). Figure 22 displays the plot of the calculated T_{Sn} versus the third-order spherical

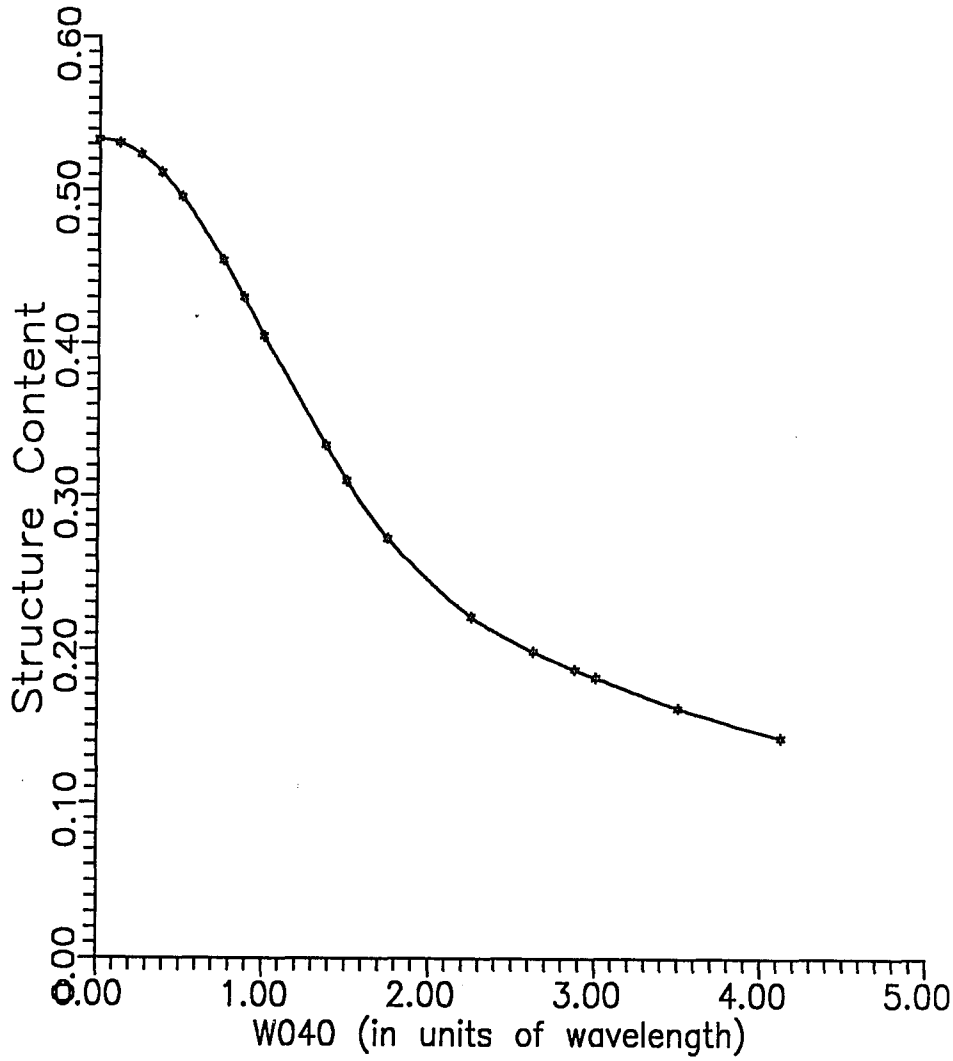

Figure 22. Structure content in the normalized optical transfer function.

aberration coefficient. The graph shows that the system's ability to reproduce fine details decreases sharply for more than a quarter-wave of aberration present. This corresponds to the drop-off in the magnitude of the transfer function at high frequencies with aberration, and agrees with our gaussian image distribution example. The drop-off in T_{sn} slows down around $W_{040}=2\lambda$. From the magnitude plots of $\mathcal{F}$ we see that the depressed region starts to form a central hump at this point ($W_{040}=2\lambda$), and accounts for the slowed rate of decrease in T_{sn}.

We fit several curves to the graph in Figure 22. The best analytical representation for the graph is the Cauchy distribution which fits the graph very well out to two wavelengths of aberration, and acts as a lower bound for larger aberrations. The graph of T_{sn} and the best fit Cauchy function is shown in Figure 23. The best fit Cauchy function is

$$f_c(x) = \frac{c}{\pi}\,\frac{b}{b^2+x^2}, \quad x=W_{040}$$
$$b = 1.79661$$
$$c = 3.01025. \tag{47}$$

Equation (47) fits the T_{sn} curve exactly at $W_{040}=0.75\lambda$.

In summary, we introduce the structure content in the normalized transfer function as a measure of the system's ability to reproduce high frequencies. For less than two waves of aberration the normalized structure content follows the Cauchy function. The formation of central humps in the depression region of the magnitude of $\mathcal{F}$ slows down the rate of decrease of the structure content when two or more waves of aberration are present. The Cauchy function in this case acts as a lower bound to T_{sn}.

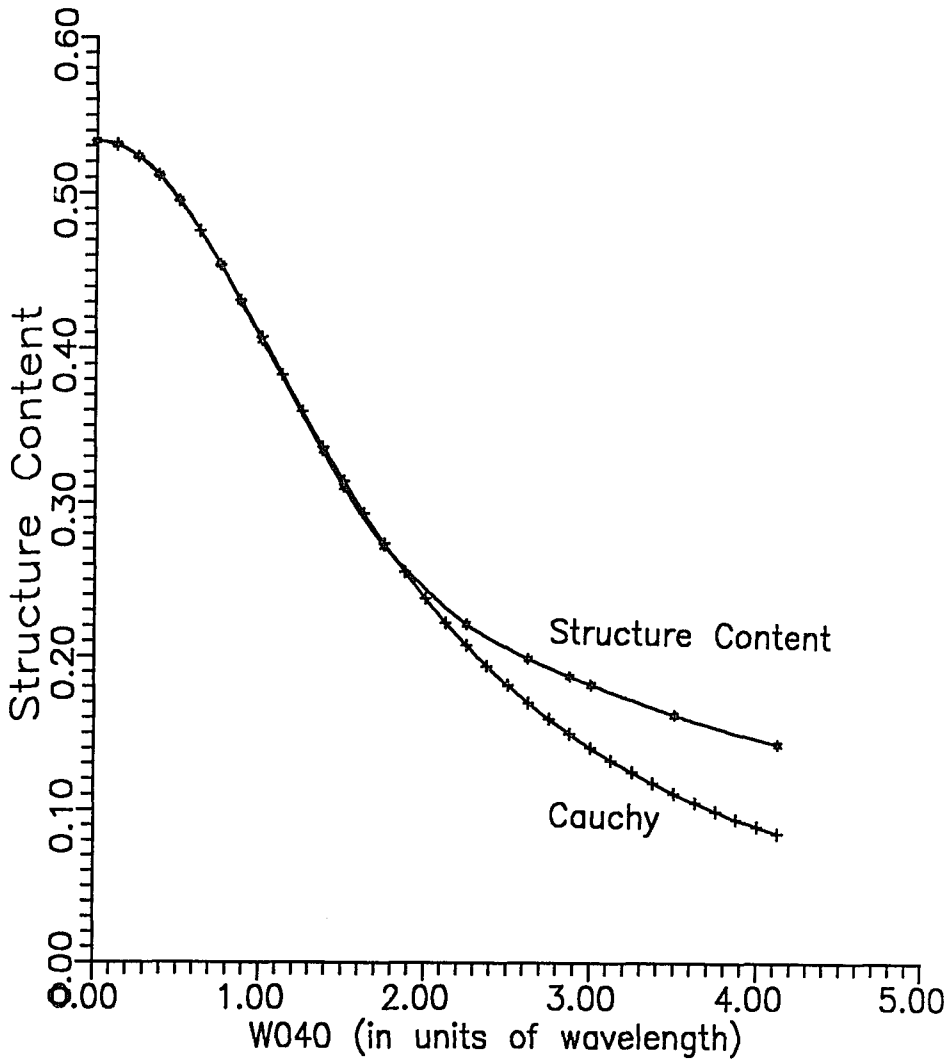

Figure 23. Structure content in $\mathscr{F}$ and the best fit Cauchy function.

IV. CONCLUSIONS

The results of this thesis has revealed several interesting features of the incoherent three-dimensional optical transfer function in the presence of third-order spherical aberration. The effect of the aberration term is generally to degrade the magnitude and introduce a phase term into the transfer function. We numerically calculated the normalized transfer function, $\mathcal{F}$, and found its magnitude to exhibit the same type of behavior as the two-dimensional transfer function. The magnitude suffers from low-pass attenuation as a function of aberration and contains oscillatory regions when more than one wave of aberration is present. Much of the degradation in the transfer function is manifest in the longitudinal frequency dependence, ω_3. The magnitude of the transfer function is the largest at ω_3=0, and the phase of the transfer function is zero here. In fact, $\mathcal{F}$ reduces to the diffraction-limited case when ω_3=0, regardless of the magnitude of spherical aberration present; see Equation (28). An heuristic argument goes as follows. By Equation (6.2a) of Frieden's paper,

$$F(\Omega) = \frac{1}{\sqrt{2\pi}} \int_{-\infty}^{\infty} d\gamma \tau(\omega;\gamma) e^{-j\omega_3 \gamma}, \tag{48}$$

where $\tau(\omega;\gamma)$ is the 2-D optical transfer function. At ω_3=0,

$$F(\omega,0) = \frac{1}{\sqrt{2\pi}} \int_{-\infty}^{\infty} d\gamma \tau(\omega;\gamma). \tag{49}$$

Combining (49) and (13), we obtain

$$\mathcal{F}(\omega,0) = \frac{\omega}{2Y_E r_G} \int_{-\infty}^{\infty} d\gamma \tau(\omega;\gamma). \tag{50}$$

Equation (50) shows that $\mathcal{F}(\omega,0)$ is proportional to the integral along the longitudinal direction of the transverse optical transfer function. Evidently, the effects of spherical aberration cancel during the $d\gamma$ integration over all longitudinal plane positions.

The phase term of $\mathcal{F}(\Omega)$ is caused by, and increases monotonically with, the longitudinal frequency. It approaches a maximum of $2\pi\left[\frac{W_{040}}{\lambda}\right]$ when the lateral frequency is equal to half of its cutoff frequency and the longitudinal frequency is at cutoff. To summarize, the effect of spherical aberration is more severe on longitudinal spatial frequency content than on lateral frequency content.

We calculate a figure of merit to characterize the effects of aberration. The structure content in the normalized transfer function is introduced as a measure of the low-pass attenuation caused by the aberration. It is well approximated by a Cauchy function for less than two waves of aberration, and is lower bounded by the Cauchy curve for larger amounts of aberration.

The next step in this analysis would be to analyze the presence of other third-order aberrations, such as coma or astigmatism. It would be interesting to see, for example, which third-order aberration most strongly affects 3-D image quality.

APPENDIX A

```
C  FSCRIPT.FOR, F(ω,ω3). Numerically (along line l) calculates the normalized 3-D
C  optical transfer function with spherical aberration, assuming a circular clear
C  pupil with radius = YE. Numerical integration uses the Jet Propulsion Lab
C  MATH 77 LIBRARY. Links with file MATH.OLB (MATH_77 LIBRARY). In link
C  command, type LINK FSCRIPT,MATH/LIB. Program uses normalized variables.
C
C
      INTEGER IOPT(2),L,M,N
      REAL A,B,ANSWER,WORK(7),PI,Y,Z,COTFMAG(32,32),COTFANG(32,32)
      REAL EXTRA,OINT,S,C(32),D(32),WC,W3C,CON,AW040(4)
      OPEN(UNIT=10,FILE='WMAG1X4.DAT',STATUS='NEW')
      OPEN(UNIT=11,FILE='WANG1X4.DAT',STATUS='NEW')
      OPEN(UNIT=12,FILE='WMAG2X4.DAT',STATUS='NEW')
      OPEN(UNIT=13,FILE='WANG2X4.DAT',STATUS='NEW')
      OPEN(UNIT=14,FILE='WMAG3X4.DAT',STATUS='NEW')
      OPEN(UNIT=15,FILE='WANG3X4.DAT',STATUS='NEW')
      OPEN(UNIT=16,FILE='WMAG4X4.DAT',STATUS='NEW')
      OPEN(UNIT=17,FILE='WANG4X4.DAT',STATUS='NEW')
C
      PI=4.0*ATAN(1.0)
C  IOPT VECTOR DENOTES OPTIONS FOR SINTF, PICK NO OPTIONS
      IOPT(2)=0
C
C  DO FOR INCREASING AMOUNTS OF SPHERICAL ABERRATION
      DO 490 L=1,4
C
C  W040 = SPHERICAL ABERRATION COEFFICIENT, IN mm
C     AW040 = SPHERIAL ABERRATION COEFFICIENT, IN wavelength =
W040/LAMDA
      AW040(L)=FLOAT(L)/4.0
C
C  SECTION TO DEFINE INTEGRATION VARIABLES TO BE PASSED TO SINTF
C
      DO 200 I=1,32
        C(I)=FLOAT(I)/32.0
              WORK(3)=C(I)**2.0
C
        DO 100 J=1,32
                D(J)=FLOAT(J)/32.0
C
C  SECTION TO CALCULATE LIMITS OF LINE INTEGRAL
     EXTRA=ABS(D(J))/4.0
                OINT=WORK(3) + EXTRA
          IF(C(I).GE.1.0.OR.OINT.GE.C(I))THEN
C      THE TWO DISPLACED PUPILS DO NOT INTERSECT
```

```
                COTFANG(I,J)=0.0
                COTFMAG(I,J)=0.0
                GOTO 100
              ELSE
      WORK(4)=EXTRA/C(I)
                WORK(5)=WORK(4)**2.0 + WORK(3)
                WORK(6)=AW040(L)*4.0*PI*D(J)
C               A = UPPER LIMIT OF INTEGRATION
C     B = LOWER LIMIT OF INTEGRATION
        S=1.0 - (C(I) + WORK(4))**2.0
        A=SQRT(S)
        B=0.0
       ENDIF
C
C  SECTION TO CALCULATE INTEGRAL FOR COTF
C  WORK(7) TELLS SINTF WHICH INTEGRAL TO DO.  1 = COSINE, 2 = SINE
       WORK(7)=1.0
       CALL SINT1 (B,A,ANSWER,WORK,IOPT)
       Y=ANSWER
       WORK(7)=2.0
       CALL SINT1 (B,A,ANSWER,WORK,IOPT)
       Z=ANSWER
C
       IF(Y.EQ.0.0)THEN
              IF(Z.EQ.0.0)THEN
                COTFMAG(I,J)=0.0
                COTFANG(I,J)=0.0
              ELSEIF(Z.GT.0.0)THEN
                COTFMAG(I,J)=Z
                COTFANG(I,J)=90.0
         ELSE
                COTFMAG(I,J)=-Z
                COTFANG(I,J)=-90.0
              ENDIF
              GOTO 100
       ENDIF
       COTFMAG(I,J)=SQRT(Y**2.0+Z**2.0)
       COTFANG(I,J)=(180.0*ATAN(Z/Y))/PI
       IF(Y.LT.0.0)COTFANG(I,J)=COTFANG(I,J)+180.0
 50     IF(COTFANG(I,J).GE.360.0)COTFANG(I,J)=COTFANG(I,J)-360.0
       IF(COTFANG(I,J).GE.180.0)COTFANG(I,J)=COTFANG(I,J)-360.0
 100   CONTINUE
C
 200  CONTINUE
C
C  SECTION TO OUTPUT DATA TO FILES
     M=L*2 + 8
     N=L*2 + 9
     WRITE(M,455)AW040(L)
 455  FORMAT(' W040/LAMDA =',F7.3)
     WRITE(M,457)
```

```
 457  FORMAT(//,' Magnitude of W*F(W,W3)')
      DO 465 I=1,32
    DO 463 J=1,32
          WRITE(M,460)C(I),D(J),COTFMAG(I,J)
 460       FORMAT(1X,F9.6,1X,F9.6,1X,F10.4)
 463     CONTINUE
 465   CONTINUE
      WRITE(N,455)AW040(L)
      WRITE(N,470)
 470   FORMAT(//,' Angle of W*F(W,W3)')
      DO 475 I=1,32
               DO 473 J=1,32
          WRITE(N,460)C(I),D(J),COTFANG(I,J)
 473     CONTINUE
 475   CONTINUE
C
C  DO FOR NEXT SPHERICAL ABERRATION COEFFICIENT
 490   CONTINUE
C
      CLOSE(UNIT=10)
      CLOSE(UNIT=11)
      CLOSE(UNIT=12)
      CLOSE(UNIT=13)
      CLOSE(UNIT=14)
      CLOSE(UNIT=15)
      CLOSE(UNIT=16)
      CLOSE(UNIT=17)
 500   STOP
      END
C
C
C
C
      SUBROUTINE SINTF(ANSWER,WORK,IFLAG)
C  SUBROUTINE SINTF.  SUBROUTINE TO PROVIDE INTEGRAND FOR SINT1.
C
      REAL ANSWER,WORK(7),X
      INTEGER IFLAG
C
      X=WORK(6)*(WORK(1)**2.0 + WORK(5))
      IF(WORK(7).EQ.1.0)THEN
               ANSWER=COS(X)
      ELSEIF(WORK(7).EQ.2.0)THEN
               ANSWER=SIN(X)
      ELSE
               TYPE*,' WORK(7) IS INVALID.  CHECK PROGRAM.'
      ENDIF
C
      RETURN
      END
```

APPENDIX B

```
C  NEWRES.FOR, numerically calculates the volume of the magnitude squared
C  of the 3-D ℱ with 3rd-order spherical aberration, assuming circular clear
C  pupil with radius = YE. Equivalent to the structure content of the transfer
C  function.  Type LINK NEWRESOL,MATH/LIB.  Program uses normalized
C  Variables.  This program normalize the actual volume by 2*YE*RG/SQRT(2*PI).
C
      INTEGER IOPT(2),L,NDIMI,NWORK
      REAL ANSWER,WORK(421),PI,AW040(40),COTFMAG(40),Y,Z
      OPEN(UNIT=10,FILE='NEWRES.DAT',STATUS='NEW')
C
C
C  SECTION TO ASSIGN CONSTANTS TO VARIABLES
C
      PI=4.0*ATAN(1.0)
C  IOPT VECTOR DENOTES OPTIONS FOR SINTF, PICK NO OPTIONS
      IOPT(2)=0
C
C  SECTION TO DEFINE INTEGRATION VARIABLES
      WORK(418)=4.0*PI
C  NDIMI = NUMBER OF DIMENSIONS OF INTEGRATION
      NDIMI=3
C  NWORK = NUMBER OF SPACES ALLOWED FOR WORK ARRAY
      NWORK=421
C
C     INITIALIZE DATA FILES
      WRITE(10,457)
 457  FORMAT(//,' W040/LAMDA   Normalized Effec. Resolution Length')
C
C  DO FOR INCREASING AMOUNTS OF SPHERICAL ABERRATION
      DO 200 L=1,40
C        AW040 = SPHERICAL ABERRATION COEFFICIENT, IN UNITS OF WAVE-
LENGTH
         AW040(L)=FLOAT(L)/8.0
         WORK(420)=AW040(L)
C
C  SECTION TO CALCULATE INTEGRALS
    TYPE *,' CALL SINTM'
    WORK(417)=1.0
        CALL SINTM (NDIMI,ANSWER,WORK,NWORK,IOPT)
    Y=2.0*ANSWER
    WRITE(6,53)WORK(1),IOPT(1)
 53     FORMAT(' ERROR ESTIMATE =',G15.6,'     STATUS FLAG =',I3,/)
    WORK(417)=2.0
        CALL SINTM (NDIMI,ANSWER,WORK,NWORK,IOPT)
    Z=2.0*ANSWER
```

```
      WRITE(6,53)WORK(1),IOPT(1)
          COTFMAG(L)=Y+Z
C
C  SECTION TO OUTPUT DATA TO FILES
          WRITE(10,460)AW040(L),COTFMAG(L)
 460      FORMAT(1X,F12.4,1X,F15.7)
C
C  DO FOR NEXT SPHERICAL ABERRATION COEFFICIENT
 200  CONTINUE
C
C
C
      CLOSE(UNIT=10)
 500  STOP
      END
C
C
C
C
C
      SUBROUTINE SINTF(ANSWER,WORK,IFLAG)
C  SUBROUTINE SINTF.  SUBROUTINE TO PROVIDE INTEGRAND FOR SINT1.
C
      REAL ANSWER,WORK(421),X,CONST,COR,DC
      INTEGER IFLAG,NDIMI
      DATA NDIMI /3/
C
      IF(IFLAG.EQ.0)THEN
C  COMPUTE INNERMOST INTEGRAND
         WORK(414)=ABS(WORK(2))/(4.0*WORK(3))
         WORK(416)=WORK(420)*WORK(418)*WORK(2)
         X=WORK(1)**2.0 + WORK(414)**2.0 + WORK(3)**2.0
    IF(WORK(417).EQ.1.0)THEN
          ANSWER=COS(WORK(416)*X)
    ELSE
          ANSWER=SIN(WORK(416)*X)
    ENDIF
      ELSEIF(IFLAG.EQ.1)THEN
C  COMPUTE LIMITS OF INNER INTEGRAND
                WORK(4)=0.0
                COR=1.0-(WORK(3)+ABS(WORK(2))/(4.0*WORK(3)))**2.0
                WORK(7)=SQRT(COR)
      ELSEIF(IFLAG.EQ.2)THEN
C  COMPUTE LIMITS OF INTEGRAND FOR D
    DC=4.0*(WORK(3)-WORK(3)**2.0)
                WORK(5)=0.0
                WORK(8)=DC
      ELSEIF(IFLAG.EQ.3)THEN
C  COMPUTE LIMITS OF INTEGRAND FOR C
                WORK(6)=0.0
                WORK(9)=1.0
```

```
      ELSEIF(IFLAG.EQ.-1)THEN
C  COMPUTE INTEGRAND FOR D
     ANSWER=ANSWER**2.0
      ELSE
C  IFLAG=-2, COMPUTE C INTEGRAND.  ANSWER=ANSWER
            RETURN
      ENDIF
C
      RETURN
      END
```

REFERENCES

1. B. R. Frieden, "Optical Transfer of the Three-Dimentional Object," J. Opt. Soc. Am. 57, 56 (1966).

2. E. Wolf, "Three-Dimensional Structure Determination of Semitransparent Objects from Holographic Data," Opt. Commun. 1, 153 (1969).

3. N. Streibl, "Three-Dimensional Imaging by a Microscope," J. Opt. Soc. Am. A 2, 121 (1985).

4. D. A. Agard, "Optical Sectioning Microscopy: Cellular Architecture in Three Dimensions," Ann. Rev. Biophys. Bioeng. 13, 191 (1984).

5. Y. Hu and B. R. Frieden, "Restoration of Longitudinal Images," Applied Optics 27, 414 (1988).

6. N. Davies, M. McCormick and L. Yang, "Three-Dimensional Imaging Systems: A New Development," Applied Optics 27, 4520 (1988).

7. N. Streibl, "Depth Transfer by an Imaging System," Optica Acta 31, 1233 (1984).

8. F. Macias-Garza, A. C. Bovik and K. R. Diller, "Missing Cone of Frequencies and Low-pass Distortion in Three-Dimensional Microscopic Images," Optical Engineering 27, 461 (1988).

9. T. N. L. Patterson, "The Optimum Addition of Points to Quadrature Formulae," Mathematics of Computation 22, 847 (1968).

10. JPL Applied Mathematics Group, *Math 77: A Library of Mathematical Subprograms for Fortran 77*, Jet Propulsion Lab D-1341 (1984).

11. M. Abramowitz and I. A. Stegun, Editors, *Handbook of Mathematical Functions*, Dover Publications, New York, pp. 300-301, 321-323 (1970).

12. R. Barakat and A. Houston, "Transfer Function of an Annular Aperture in the Presence of Spherical Aberration," J. Opt. Soc. Am. 55, 538 (1965).

13. E. H. Linfoot, *Fourier Methods in Optical Image Evaluation*, Focal Press, London, p. 33 (1966).

14. T. S. Huang, Editor, "Picture Processing and Digital Filtering," Topics in Applied Physics 6, Springer-Verlag, New York, p. 210 (1979).